To the Graduate Council:

I am submitting herewith a thesis written by Brian F. Hasson entitled "THE PRODUCTION OF HIGH RYDBERG STATES OF THE PROJECTILE IN COLLISIONS OF 0.1 MeV/u Ag^{4+} IONS WITH Ar GAS TARGETS." I have examined the final copy of this thesis for form and content and recommend that it be accepted in partial fulfillment of the requirements for the degree of Master of Science, with a major in Physics.

Marianne Breinig
Dr. Marianne Breinig, Major Professor

We have read this thesis and recommend its acceptance:

Leo L. Ratliff

Stuart B. Elston

Accepted for the Council:

C. W. Minkel
Associate Vice Chancellor
and Dean of the Graduate School

THE PRODUCTION OF HIGH RYDBERG STATES OF THE PROJECTILE IN COLLISIONS OF 0.1 MeV/u Ag^{4+} IONS WITH Ar GAS TARGETS

A THESIS PRESENTED FOR THE

MASTER OF SCIENCE DEGREE

THE UNIVERSITY OF TENNESSEE, KNOXVILLE

BRIAN FITZGERALD HASSON

DECEMBER 1991

DEDICATION

This Masters thesis is dedicated to my wife Kathleen, for her never ending love and understanding, to my mother Alix Hasson, my younger brother Donald, to the rest of my family, and my wife's family. Without any one of them the job of completing this Masters thesis may have overwhelmed me, and I may have faltered in accomplishing this goal.

I also dedicate this thesis to Dr. Tricia Reeves, who recommended that I attend Graduate school, and finally to both Kathy McCown and Mr. and Mrs. Wilson for their true friendship in good times and bad.

ACKNOWLEDGMENTS

I would like to especially thank my major Professor Marianne Breinig for her everlasting support and advice on this project and life itself, as well as C.J. Gaither for all his help on the computers and the experiments we have run, and Roy Buhl for his help in machining parts for the apparatus. In addition, I would like to say thank you to all the U.T. Atomic Physics group members at Oak Ridge for making this a very satisfying, as well as a fun place to work and learn.

I would like to send a special thank you to Professor Lee Riedinger and Professor Stu Elston for taking the time away from their busy schedules to be members of my defense committee. Also I would like to thank Professor Bob Lyde for his continual support while at Tennessee.

Finally I would like to thank my wife Kathy for her support throughout my studies.

ABSTRACT

This experiment concerns the study of inelastic processes at intermediate collision velocities which produce high Rydberg states of the projectile ion. We investigate the production processes which create these highly excited states for 0.1 MeV/u Ag^{4+} ions colliding with an argon gas target by detecting stripped Rydberg electrons in coincidence with exit core charge states, 3+, 4+, 5+, and 6+ of the projectile ion.

The goal of this experiment is to measure the Rydberg electron production cross sections for projectile Rydberg electrons with energies lying in specified energy intervals. The production cross sections are measured for target electron capture to high Rydberg states of the projectile with and without an additional bound state capture, and for projectile electron excitation to high Rydberg states with and without additional projectile electron ionization. The production cross sections for these events are used to determine if the n-state distribution of these high Rydberg states depends on the production process. Field ionization techniques are used to strip the Rydberg electrons from the cores of the projectile ions, and standard coincidence methods are employed to determine if a detected Rydberg electron is stripped from a particular ion.

The Rydberg electron production cross sections per unit

energy interval are found to be on the order of 10^{-17} cm^2/eV. The production cross section ratios per unit energy interval for electrons stripped from the highest lying Rydberg states compared to electrons stripped from somewhat lower lying Rydberg states are found to be noticeably different for capture processes as opposed to excitation processes. Thus, the n-state distribution of these Rydberg electrons depends on the production mechanisms, i.e. it is different for Rydberg states that are formed by target electron capture events than for Rydberg states that are formed by projectile electron excitation events. However, no dependence of the n-state distribution on the number of active electrons involved in the production process is found.

TABLE OF CONTENTS

LIST OF TABLES

LIST OF FIGURES

LIST OF ABBREVIATIONS

Independent Electron Model	IEM
Argon	Ar
Silver	Ag
Channel Electron Multiplier	CEM
Multichannel Analyzer	MCA
Multichannel Scaler	MCS
Analog to Digital Convertor	ADC
Nuclear Instrumentation Modules	NIM
Single Channel Analyzer	SCA
Transistor - Transistor Logic	TTL
Counter/Timer	CT
Digital to Analog Convertor	DAC
Time to Amplitude Convertor	TAC
Electron Loss to the Continuum	ELC
Electron Capture to the Continuum	ECC
High Voltage Terminal	HV

CHAPTER 1

INTRODUCTION

In a collision between a projectile ion and a target gas atom projectile electrons may be excited, or target electrons may be transferred, into high lying bound states of the projectile ion. These bound states are called high Rydberg states of the ion, and the electrons in these states are referred to as Rydberg electrons. In order for these high Rydberg states to be produced the collision must be inelastic, allowing for energy transfer between the projectile ion and the target gas atom. The most probable events occurring during a collision are single electron transitions such as target and projectile single excitation and ionization, and single target electron capture by the projectile. Events that are less probable are multiple electron transitions involving more than one active electron.

The relative velocity, v_c, between the projectile and the target is categorized according to its magnitude relative to the speed of the electrons, v_e, which are active in the collision. For fast collisions $v_c > v_e$, and elastic processes dominate in the collision. For fast collisions the Born approximation is often used to calculate transition cross sections.[1] For slow collisions $v_c < v_e$, and inelastic

collisions dominate. Here the Born-Oppenheimer separation of the ionic and electronic motion is possible when calculating transition probabilities.[2] For intermediate velocity collisions $v_c \sim v_e$, and inelastic processes become more important.

This experiment concerns the study of inelastic processes at intermediate collision velocities which produce highly excited bound states of the projectile ion near the ionization threshold. We are investigating the production processes which create these highly excited states for 0.1 MeV/u Ag^{4+} ions colliding with an argon gas target by detecting stripped Rydberg electrons in coincidence with the exit core charge states, 3+, 4+, 5+, 6+, and 7+ of the projectile ion. Exit core charge states 4+ and 5+ are associated with single electron events, where

4+: single target electron capture to a high Rydberg state

5+: single projectile electron excitation to a high Rydberg state.

Exit core charge states 3+ and 6+ are associated with events which involve two active electrons, where

3+: target electron capture to a high Rydberg state and capture to a lower lying bound state

6+: projectile electron excitation to a high Rydberg state and projectile ionization.

Our goal is to determine the n-state distribution of

these Rydberg electrons in the post collision ions for the various production processes, and to find out if the n-state distribution depends on the production process. Field ionization techniques are employed to strip the Rydberg electrons from the cores of the ions, and standard coincidence methods are used to determine if a detected Rydberg electron is stripped from a particular ion.

A. RYDBERG ELECTRONS

Rydberg atoms (or ions) are highly excited atoms (or ions) with at least one electron occupying a state in the atom (or ion) with large principle quantum number n. The electrons in these states are said to be in a Rydberg state of the atom (or ion). Highly excited Rydberg states of atoms have been studied extensively in recent years because of their unique properties; they are quite stable against radiative decay, are highly reactive to charged particles and to external fields due to their weak binding, and have a large electron cloud.[3] For high Rydberg states the density of states dn/dE, varies as n^3, they have long life times that scale as n^3, and they have low ionization thresholds.[4] Single electron excitation and capture cross sections to states with high principal quantum numbers,[5] n, scale as $\sim n^{-3}$. Any atom can be made into a Rydberg atom by promoting one or more of its bound electrons to a very high energy level.[6] Rydberg atoms are very large in size, some

having diameters on the order of 0.01 mm.

If we consider a Rydberg ion as a core with a nucleus surrounded by tightly bound electrons and one electron that travels at a large distance (Rydberg electron), then the effective potential seen by the Rydberg electron is nearly Coulombic. The potential seen will be Coulombic as long as the orbit of the Rydberg electron does not penetrate the core, which is ~ 1 a.u. in radius, centered at the nucleus. Therefore, to a good approximation, the Rydberg electron can be described by the wave function which describes a Rydberg electron in a hydrogenic ion. The expression for the Rydberg electron energy is modified from that of an electron in a hydrogenic ion, and is expressed in terms of an effective quantum number μ in atomic units[4]

$$E = -1/2 \cdot (Z^2/\mu^2) \text{ a.u.} \qquad (1.1)$$

The difference between the effective principle quantum number and the hydrogenic principle quantum number is called the quantum defect. The quantum defect provides a measure of the difference between the actual potential and a pure Coulomb potential as seen by the Rydberg electron. It depends on the overlap of the orbits of the Rydberg electron and the core electrons. For large Rydberg electron orbits $\mu \sim n$, and the principal quantum number n is used to determine the Rydberg electron energy.

Electrons in high Rydberg states of the projectile and electrons in low lying continuum states of the projectile

are considered to be closely related as pointed out by Macek and Rudd[7]. In fact electron loss to the continuum (ELC) is suggested to be the asymptotic limit of successive excitations to higher Rydberg orbits until the electron becomes unbound[8]. It is also thought that electron capture to the continuum (ECC) is the asymptotic limit of the process of electron capture to Rydberg states of increasing energy. The excitation and capture cross sections as a function of electron energy continue smoothly across the ionization threshold (see fig. 1.1).

In fast ion-atom collisions electron capture processes to high Rydberg and continuum states of the projectile involve a large momentum transfer to the captured electron and require a close collision. In contrast, projectile excitation and ionization into low lying continuum states involve a small momentum transfer to the active electron and is likely to happen at larger impact parameters.

B. RECENT DEVELOPMENTS

The independent electron model (IEM) has been used very successfully to describe most single electron and some multiple electron transitions in ion-atom collisions. The IEM assumes that each electron moves in an effective potential composed of the potentials of the positively charged nuclei and the average potential of all the other electrons in the ions. Consequently, the IEM neglects

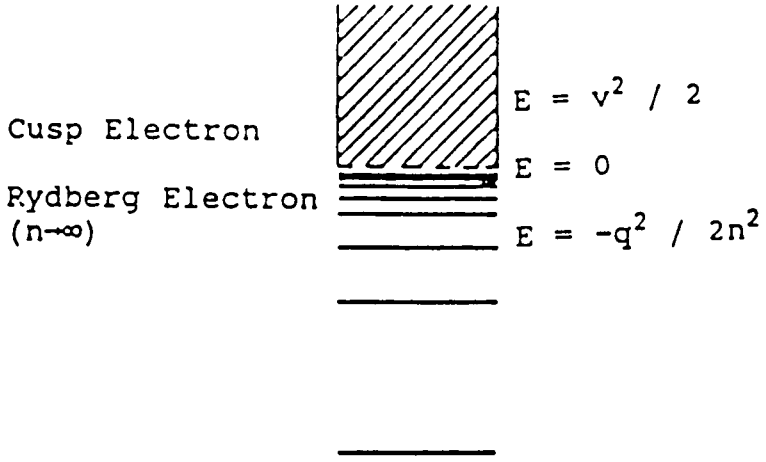

FIGURE 1.1 CUSP AND RYDBERG STATES IN ONE ELECTRON SPECTRA

electron correlation,[9] which is the difference in the average and the exact electron-electron Coulombic interactions.

Double electron events in ion-atom collisions have received considerable attention in recent years. Some of the events that are currently being studied are double ionization of the target,[10] simultaneous ionization of the target and target electron capture by the projectile,[11] and the production of doubly excited projectile states.[12] The description of these events relies heavily on the understanding of how electrons are ionized, and how excited states are formed and populated in multiple electron events. It may turn out that the IEM is not an adequate model for describing these events.

McGuire[13] has determined that at moderately high

velocities the IEM gives reasonable results for multiple inner-shell ionization. In contrast to McGuire's findings recent studies of multiple ionization of the target atom with various collision systems at intermediate and fast collision velocities have revealed the importance of electron-electron interactions.[14-18] It has been found that correlation effects play a dominant role in studies of outer-shell multiple ionization for collisions of fast protons incident on He, H, and Ar.[15,16] Tanis et al.[19] have examined electron correlation contributions during double capture in fast collisions of 3.5 MeV/u Ne^{10+} projectiles incident on Ar gas targets and found a larger probability for bound state capture accompanying Rydberg state capture than can be accounted for by the IEM. Contrary to McGuire's[13] findings, these findings[19] infer that the electron-electron interactions may contribute significantly to inner shell ionization at high collisional velocities.

At lower collision velocities McGuire[9] suggests that the correlation effects due to electron-electron interactions do not contribute significantly to the probability amplitudes. However, for two electron processes at low collisional velocities deviations from the predictions of the IEM due to electron correlation have been determined.[20] In a recent experiment Stolterfoht et al.[20] examine the production processes for the population of high Rydberg states of the projectile for double electron capture

in low energy collisions of O^{6+} with He. They found strong evidence suggesting the population of high Rydberg states in slow collisions is directly associated with electron correlation. These findings deviate from the expected production processes determined by the IEM.

In this experiment we are investigating the n-state distribution of electrons in high Rydberg states of the projectile ion created by an ion-atom collision, with $v_c \approx v_e$. From this collision we want to determine two factors. First, we want to measure the Rydberg electron production cross sections for one-electron and multi-electron transitions. Secondly, we want to determine if the n-state distribution depends on the production processes, i.e., if it is different for capture or loss events and for one-electron or two-electron events. If we determine that a difference in the n-state distribution does exist between one-electron and two-electron events, then it may be necessary to take into account correlation effects when describing ion-atom collisions at intermediate energies. If a difference does exist then the correlation effects involved in the collision would warrant further theoretical investigation.

C. FIELD IONIZATION

Electric field ionization is a very efficient method of stripping electrons from high Rydberg state of atoms and

ions, in order to detect these electrons. The details of a theoretical description of field ionization differ according to whether the system is "hydrogenic" or "nonhydrogenic"[21]. If we consider an isolated hydrogenic atom, then the energy of an electron in an eigenstate of the Hamiltonian is given by

$$E_n = -(mZ^2e^4) \; / \; (2\hbar^2n^2), \tag{1.2}$$

where m is the reduced mass, Z is the nuclear charge of the atom, n is the principal quantum number of the eigenstate, and $e^2 = q_e^2/(4\pi\epsilon_0)$. In terms of the Bohr radius $a_0 = \hbar^2/me^2$, the energy can be rewritten as

$$E_n = -(Z^2e^2) \; / \; (2a_0n^2) \tag{1.3}$$

or in terms of atomic units of energy e^2/a_0

$$E_n = -Z^2 \; / \; 2n^2. \tag{1.4}$$

If we place a hydrogenic atom in an external electric field of strength F directed along the z-axis, then to first order the eigenenergies of the electron will be given by

$$E = -(Z^2/2n^2) + (3F/2Z)\cdot n(n_1 - n_2) \quad \text{a.u.}, \tag{1.5}$$

where F is given in atomic units, and n, n_1, n_2, and m_0 are parabolic quantum numbers with

$$n = n_1 + n_2 + |\, m_0 \,| + 1. \tag{1.6}$$

The electric field partially removes the degeneracy of the eigenstates that have the same principal quantum number n. The energy levels that correspond to the same n split and slightly shift. This effect is known as the Stark effect, and was first studied by Johannes Stark in 1913.[22]

In an isolated hydrogen atom a degenerate state with principal quantum number n may be viewed as a linear superposition of eigenstates with a permanent dipole moment p, but different components p_z. In an external electric field of strength F in the z-direction, states with different p_z have different energies. The energy of a dipole in this field is given by

$$\mathscr{E} = -p_z F. \tag{1.7}$$

Thus, in an electric field the eigenstates with the same n but different p_z are no longer degenerate. From (eq. 1.7) we can see that the difference in energy between eigenstates with different p_z is proportional to F. This effect is called the linear Stark effect.

In addition, the electric field exerts forces on the nucleus and the electron of a hydrogenic ion in the field. These forces act on the nucleus and the electron in opposite directions due to their opposite charge. Therefore, the ion becomes polarized and acquires a small induced dipole moment which is proportional to F. The energy of each sublevel of the ion gets shifted by a small amount which is proportional to F^2. This is called the quadratic Stark effect.

Let us consider an ion of nuclear charge Z with a single electron in an electric field of strength F directed along the z-axis. The potential energy of the electron in the ion is given by

$$U(r) = -(Ze^2/r) + q_e F z. \tag{1.8}$$

U(r) has a saddle point on the z-axis at

$$z = -[(Zq_e)/(4\pi\epsilon_0 F)]^{1/2} \qquad (1.9)$$

and the potential energy of an electron at the saddle point is

$$U(z) = -q_e \cdot [(Zq_e F)/(\pi\epsilon_0)]^{1/2}. \qquad (1.10)$$

Using a classical approximation, all electrons with total energy E greater than U(z) will be in the continuum, and all electrons with $E < U(z)$ will be bound to the ion (see fig. 1.2). In a quantum mechanical treatment all energy levels of the ion are unstable and there is a probability that electrons will tunnel through the potential barrier presented by the saddle point. However, the tunneling rates fall off rapidly as the total energy of the electron falls below U(z). This leads to the idea of a "threshold field" for ionization that the classical model for ionization predicts.[23]

If we neglect the Stark effect, the total energy of an electron in an eigenstate of the ion with principal quantum number n is given by (eq. 1.4). The electron will be ionized by the field F if $E_n > U(z)$. If we set (eq. 1.4) greater than (eq. 1.10) and solve for the principal quantum number n we will have

$$n^4 > (q_e^5 Z^3 m^2)/(16 \cdot (4\pi\epsilon_0)\hbar^4 F). \qquad (1.11)$$

Thus, for a given electric field of strength F all electrons in quantum states with principal quantum numbers $n_i \geq n$ will be ionized.

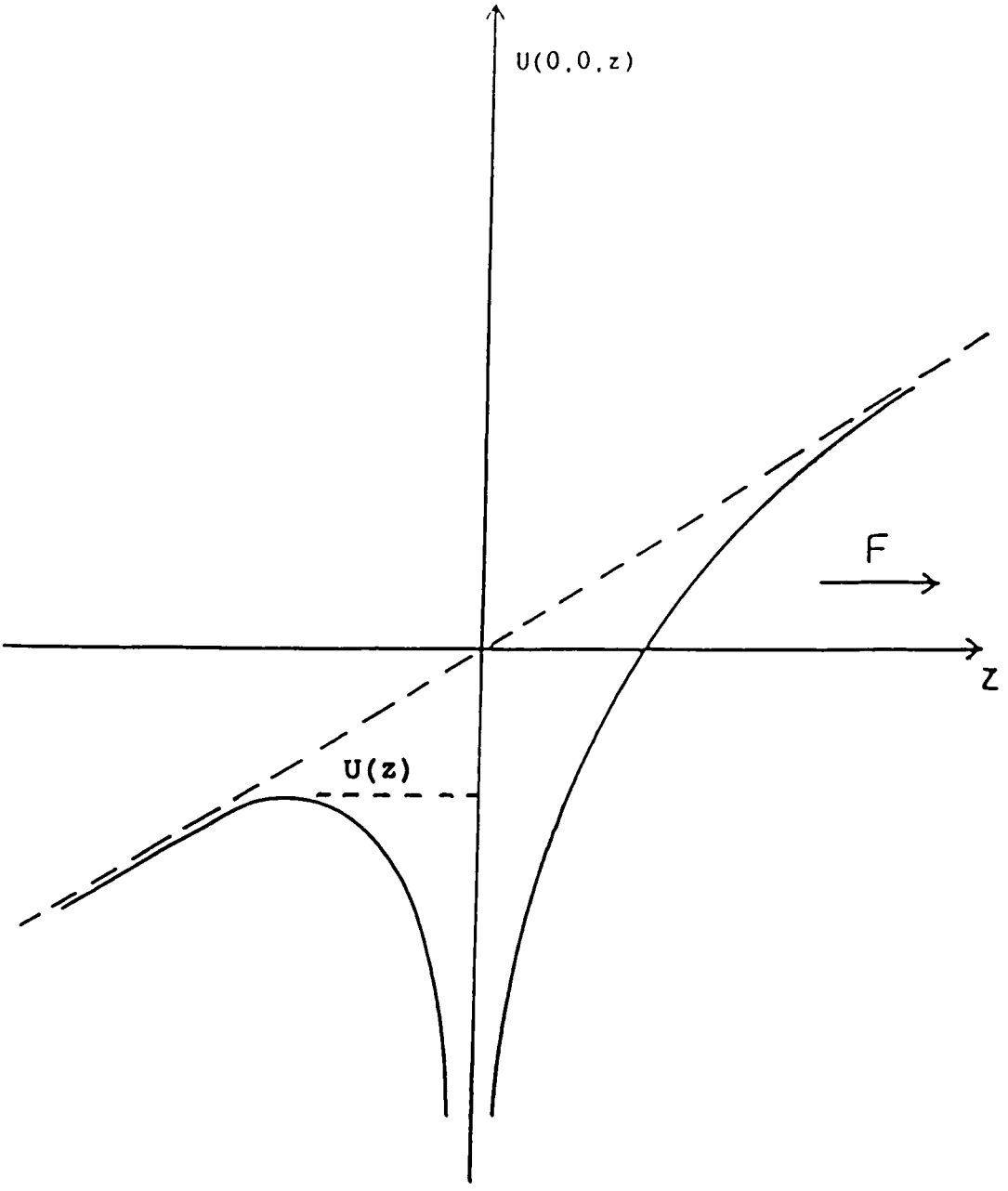

FIGURE 1.2 POTENTIAL ENERGY OF AN ELECTRON IN THE FIELD OF A BARE ION OF NUCLEAR CHARGE Z AND AN EXTERNAL ELECTRIC FIELD (F) DIRECTED ALONG THE Z-AXIS

CHAPTER 2

EXPERIMENTAL APPARATUS AND DATA ACQUISITION

We generate a 0.1 MeV/u Ag^{4+} ion beam using the EN Tandem Van de Graaff accelerator at the Oak Ridge National Laboratory. Momentum and charge state of the ions are magnetically selected, and the beam is tightly collimated before entering the experimental chamber.

In the chamber the beam interacts with target atoms in a gas cell which is mounted on the front of a 30 degree parallel plate electrostatic analyzer. The homogeneous electric field in the analyzer deflects electrons that travel with an ion, but are not bound to the ion, out of the path of the ion. After exiting through an aperture in the back of the 30 degree analyzer the ion beam transverses a short field free region before entering an electrostatic spherical sector ionizer. The radially symmetric inhomogeneous electric field in the ionizer strips electrons in high Rydberg states of the ion. Because these Rydberg states have long radiative lifetimes, scaling as $\sim n^3/Z^4$, they will not decay in the time interval it takes the beam to transverse the apparatus.[24] A projectile Ag ion will pass through the entire apparatus in approximately 0.1 μs. We estimate the lifetime of an $n \geq 60$ Rydberg state of Ag^{q+}, where q+ is the exit core charge state, to be on the order

of, or greater than 10 μs, by scaling the lifetime of the n = 10 state of hydrogen. Thus, the Rydberg states of the projectile ions in this experiment will not spontaneously decay before the beam exits the ionizer. The ions and the now free electrons exit through an aperture in the back plate of the ionizer, and then enter a 160 degree electrostatic spherical analyzer. The field in the analyzer deflects electrons of a particular energy along a circular orbit into a channel electron multiplier for detection. The stripped ion beam passes through the analyzer undeviated, before entering a long field free region (see fig. 2.1).

Further downstream the ion beam enters a charge state analyzer. The electric field in the analyzer deflects ions of a selected charge state into a multidynode detector.

A. TANDEM VAN DE GRAAFF ACCELERATOR

Ag^{-1} ions are produced by sputtering cesium ions onto a silver probe tip. The cesium ions lower the work function at the surface of the probe, thus allowing silver ions to become dislodged from the probe. Once free from the probe surface the Ag^{-1} ions are accelerated to 110 keV and momentum analyzed by a 30 degree magnet before entering the acceleration tubes.

The ion source is held at negative high voltage and the entrance to the accelerator is held at ground potential. The negative ion beam is accelerated towards the positive HV

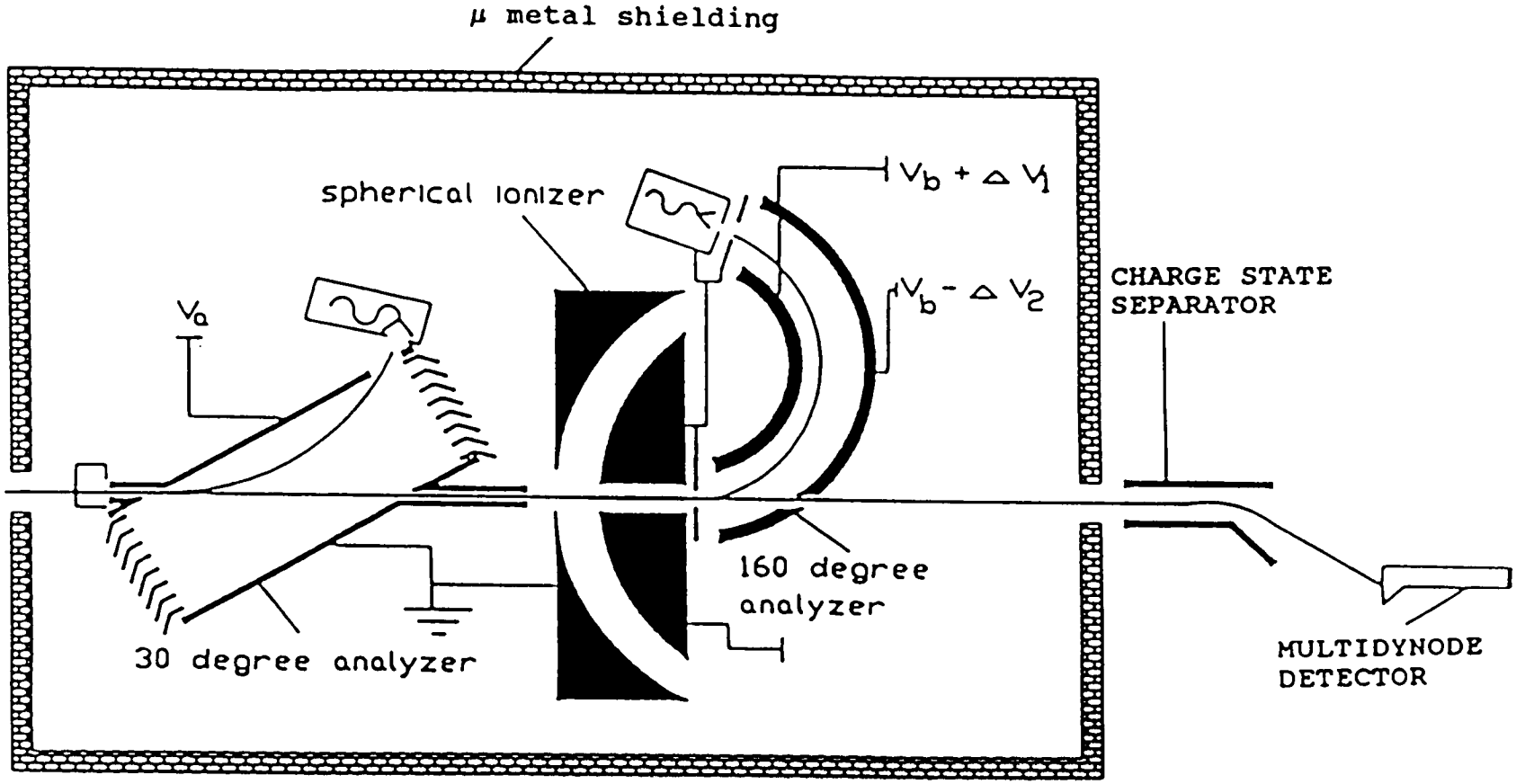

FIGURE 2.1 SCHEMATIC DIAGRAM OF THE EXPERIMENTAL APPARATUS

terminal of the EN Tandem accelerator. At the HV terminal an Ar gas stripper is used to strip the negative silver ions into a variety of positive charge states. These positive silver ions are accelerated towards the exit of the accelerator which is held at ground potential.

Upon exiting the accelerator the ions are focussed, using a quadrupole magnet, into a 90 degree analyzing magnet where only ions of a selected charge to momentum ratio are transmitted. In our experiment only 0.1 MeV/u Ag^{4+} ions of atomic mass 107 are transmitted. After traveling through a short field free region a 90 degree switching magnet directs the 0.1 MeV/u Ag^{4+} ions into the beamline preceding our experimental chamber (see fig. 2.2).

B. EXPERIMENTAL BEAMLINE

The Ag^{4+} ion beam exits the switching magnet of the accelerator and is directed down the beamline towards the experimental chamber. Before it reaches the chamber and the experimental apparatus it is collimated by two collimators that are 3/4 mm in diameter and separated by a distance of 1.36 m. The two collimators insure an angular spread of less than 1.2 mrad, and a beam spot of less than 1.2 mm in diameter on target. The residual gas pressure in this section of the beamline is $\leq 3 \cdot 10^{-7}$ torr maintained by a cryogenic pump and a diffusion pump.

After the ion passes through the second collimator it

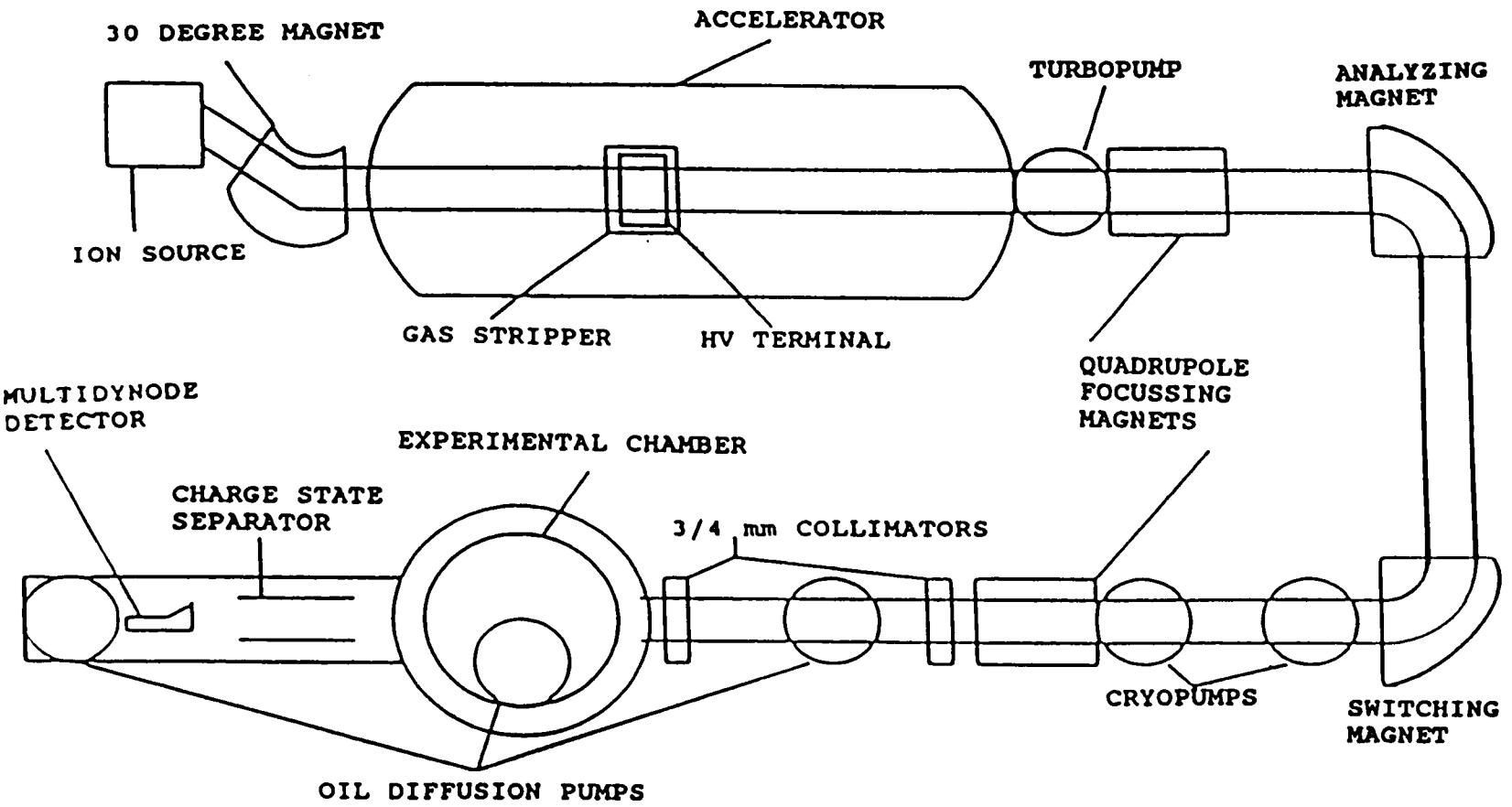

FIGURE 2.2 SCHEMATIC DIAGRAM OF EN TANDEM VAN DE GRAAF ACCELERATOR AND EXPERIMENTAL BEAMLINE

travels 22 cm before entering the experimental chamber. The chamber contains a μ-metal box (40 cm × 9 cm x 28 cm) with 3.0 cm diameter entrance and exit apertures. The μ-metal shields our apparatus from stray magnetic fields. The residual gas pressure in the experimental chamber is $\leq 5 \cdot 10^{-7}$ torr maintained by a single diffusion pump.

After exiting the experimental chamber the ion beam enters a large diameter straight section containing the charge state analyzer, the multidynode detector, and the Faraday cup. A diffusion pump maintains a pressure of $\leq 4 \cdot 10^{-7}$ torr in this section of the beamline.

C. GAS CELL

Our gas cell is 1.43 cm long and has 1.5 mm entrance and exit apertures. During the experiment gas streams out of the cell through the apertures. We therefore assume an effective gas cell length equal to the sum of the actual gas cell length and the diameters of the two apertures. The effective gas cell length is 1.73 cm. The Ar gas pressure in the cell is maintained by a flow rate controller and the pressure is monitored by a Baratron manometer. The Baratron manometer uses a diaphragm type variable capacitor to measure pressure. It compares an unknown pressure to a reference pressure.

During the experiment the manometer is used to monitor the pressure in the tube that feeds into the gas cell. This

pressure is proportional to, but not equal to, the pressure in the gas cell. During the experiment we only know the relative pressure in the cell. The actual pressure in the gas cell is obtained from the measurement of the Ag^{q+} exit charge state fractions for a Ag^{4+} beam passing through the cell. The charge exchange cross sections $\sigma(4 \rightarrow q)$ are known from a previous experiment[12] and are used in determining the actual gas pressure in the cell.

D. 30^0 PARALLEL PLATE ELECTROSTATIC ENERGY ANALYZER

The 30^0 parallel plate analyzer consists of two parallel plate electrodes held a distance d = 6.35 cm apart. The potential difference between the plates is V_p. The field between the plates,

$$F = V_p / d \quad (V/cm), \tag{2.1}$$

deflects free electrons emerging from the gas cell into the region between the plates along a parabolic trajectory away from the beam direction. Electrons bound to an ion will also feel a force due to the electric field. Electrons in very high Rydberg states of the projectile ion may be ionized in the field between the plates of the 30^0 analyzer. In this experiment the potential difference between the plates is 20 V, resulting in an electric field of strength 3.14 V/cm. The field is strong enough to prevent free electrons from exiting through the back aperture of the analyzer. Yet, the field is weak enough to only strip

electrons in the highest Rydberg states of the projectile ions (see table 2.1).

E. ELECTROSTATIC SPHERICAL SECTOR IONIZER

The ionizer consists of two concentric spherical sectors of radii r_i and r_o, for the inner sector and outer sector respectively. The outer sector is grounded while the inner sector is raised to an operating voltage V_i. The resulting electric field between the sectors is a radially symmetric inhomogeneous field with field strength

$$F(r) = V_i \cdot r_o \cdot r_i \; / \; ((r_o - r_i) \cdot r^2). \qquad (2.2)$$

An ion entering the ionizer passes through a 0.4 cm aperture in the outer sector and exits through a 0.3 cm aperture in the inner sector. The dimensions of the ionizer are shown in figure 2.3. When an ion enters the ionizer it will encounter a field of strength

$$F = 0.33 \cdot V_i \quad (V/cm). \qquad (2.3)$$

TABLE 2.1

LOWEST N-LEVELS IONIZED ($n_{30}(F)$) BY THE FIELD F IN THE 30^0 PARALLEL PLATE ELECTROSTATIC ANALYZER

q	n_{30}(3.14 V/cm)
3	229
4	284
5	336
6	385
7	433

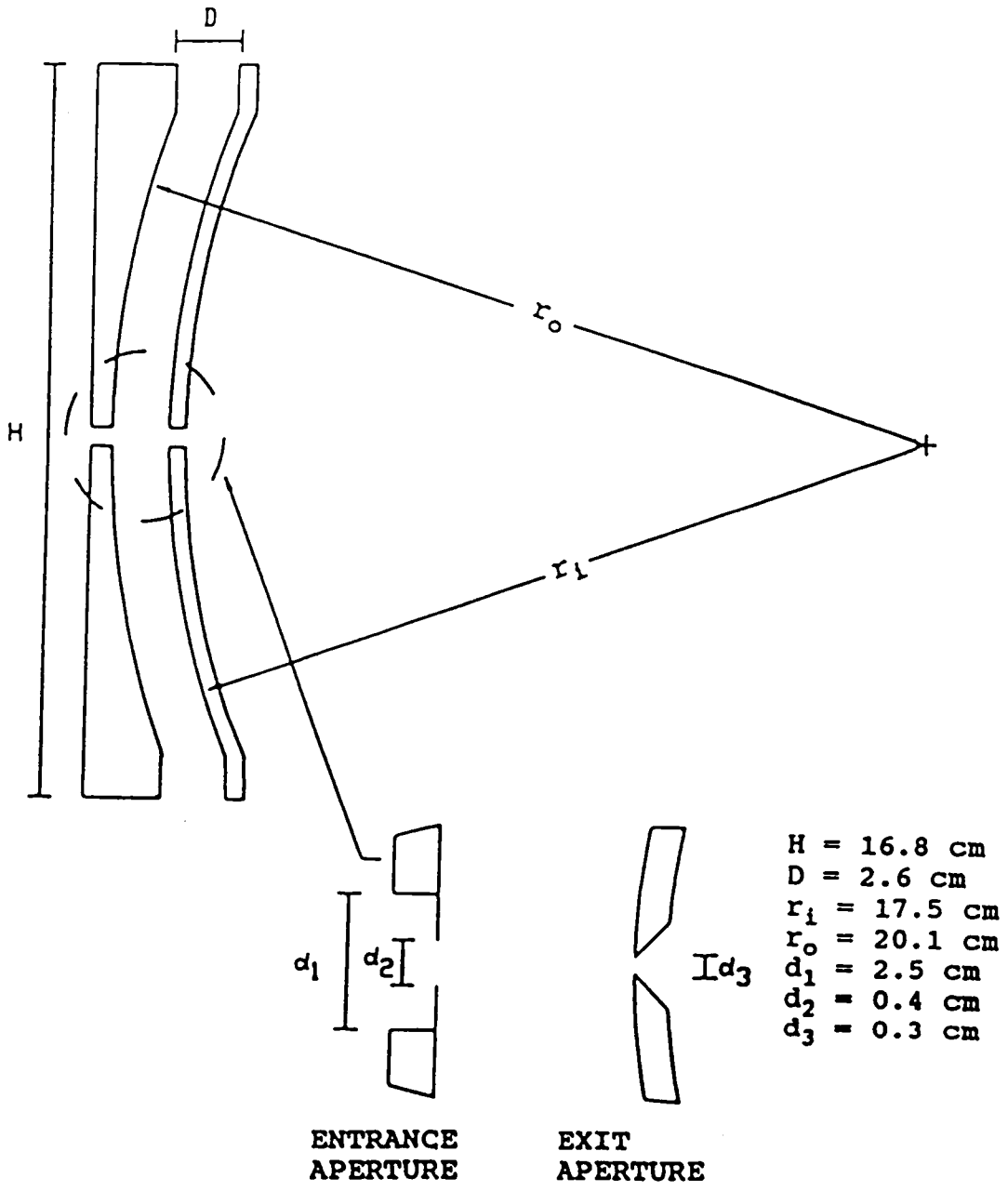

FIGURE 2.3 CROSS SECTION THROUGH THE SPHERICAL SECTOR IONIZER ALONG THE BEAM DIRECTION

Further into the ionizer the field strength increases and reaches its maximum value,

$$F = 0.44 \cdot V_i \quad (V/cm), \tag{2.4}$$

at the face of the inner sector.

When an ion is placed in a strong electric field, electrons in high lying bound states of the ion may be stripped from the core. This process is called field ionization, as discussed earlier. If we assume classical field ionization, neglecting the Stark effect and quantum mechanical tunneling, then all electrons with quantum numbers, n, $n_{30} \geq n \geq n_c$ will be ionized. We use the classical formula for a hydrogenic ion,

$$n_c^4 = 3.2 \cdot 10^8 \cdot q^3 \; / \; F, \tag{2.5}$$

to determine n_c. Here F is in V/cm, and q is the core charge state of the ion.

When the ion beam enters the spherical ionizer all electrons in levels with $n_{30} \geq n > n_c(F(r_0))$ will be stripped (see tab. 2.2). As the ion beam penetrates further into the field of the ionizer electrons in lower lying n-states will be ionized, since the strength of the electric field is increasing. The stripped electrons will be accelerated by the electric field between the two sectors towards the center of the two spheres. As the electrons accelerate they will gain kinetic energy. Electrons in lower lying n-states, which are stripped deeper in the ionizer will gain less kinetic energy than the electrons

TABLE 2.2

LOWEST N-LEVELS (n_c) IONIZED AT THE ENTRANCE OF THE IONIZER WITH 500 V AND 1000 V ACROSS THE IONIZER, RESPECTIVELY

q	$n_{c(500)}$	$n_{c(1000)}$
3	85	71
4	106	88
5	125	105
6	143	120
7	160	135

that are stripped at the entrance of the ionizer. The energy gain is given by

$$\Delta T(r) = e \cdot V_i \cdot r_o \cdot r_i \cdot (1/r_i - 1/r) \; / \; (r_o - r_i). \qquad (2.6)$$

Therefore electrons stripped at r will exit the ionizer with kinetic energy

$$T(r) = 54.4 \text{ eV} + \Delta T(r). \qquad (2.7)$$

During the experiment the inner sector of the ionizer is raised to 1000 V or 500 V while the outer sector is grounded. Table 2.3 lists the lowest n-levels stripped at the exit of the ionizer for each exit core charge state at each ionizer voltage.

F. 160^0 SPHERICAL SECTOR ELECTROSTATIC ENERGY ANALYZER

The spherical sector analyzer, first introduced by Purcell,[25] consists of concentric sectors of spherical copper surfaces. When used as an electron energy analyzer, the inner sector has a positive potential

TABLE 2.3

LOWEST N-LEVELS (n_i) STRIPPED AT THE EXIT OF THE SPHERICAL SECTOR IONIZER, WITH 500 V AND 1000 V ACROSS THE IONIZER, RESPECTIVELY

q	$n_{i(500)}$	$n_{i(1000)}$
3	79	67
4	98	83
5	116	98
6	133	112
7	150	126

$$V_{in} = \Delta V \cdot s_o \; / \; (s_i + s_o) \qquad (2.8)$$

and the outer sector has a negative potential

$$V_{out} = -\Delta V \cdot s_i / (s_i + s_o), \qquad (2.9)$$

where ΔV is the potential difference across the sectors, s_o is the radius of the outer sector, and s_i is the radius of the inner sector (see fig. 2.4). With the voltage divided in this way, electrons moving along the central ray enter at ground potential. Free electrons are deflected by the radial electric field

$$F_s(r) = \Delta V \cdot s_i \cdot s_o / ((s_o - s_i) \cdot r^2) \qquad (2.10)$$

between the sectors. The field will only deflect electrons in a certain energy band through the exit aperture of the analyzer.

In general an analyzer is asked to accept a beam of charged particles which is diverging in two directions at the entrance. Angles α in the deflection plane and β in the plane perpendicular to deflection, are measured from the

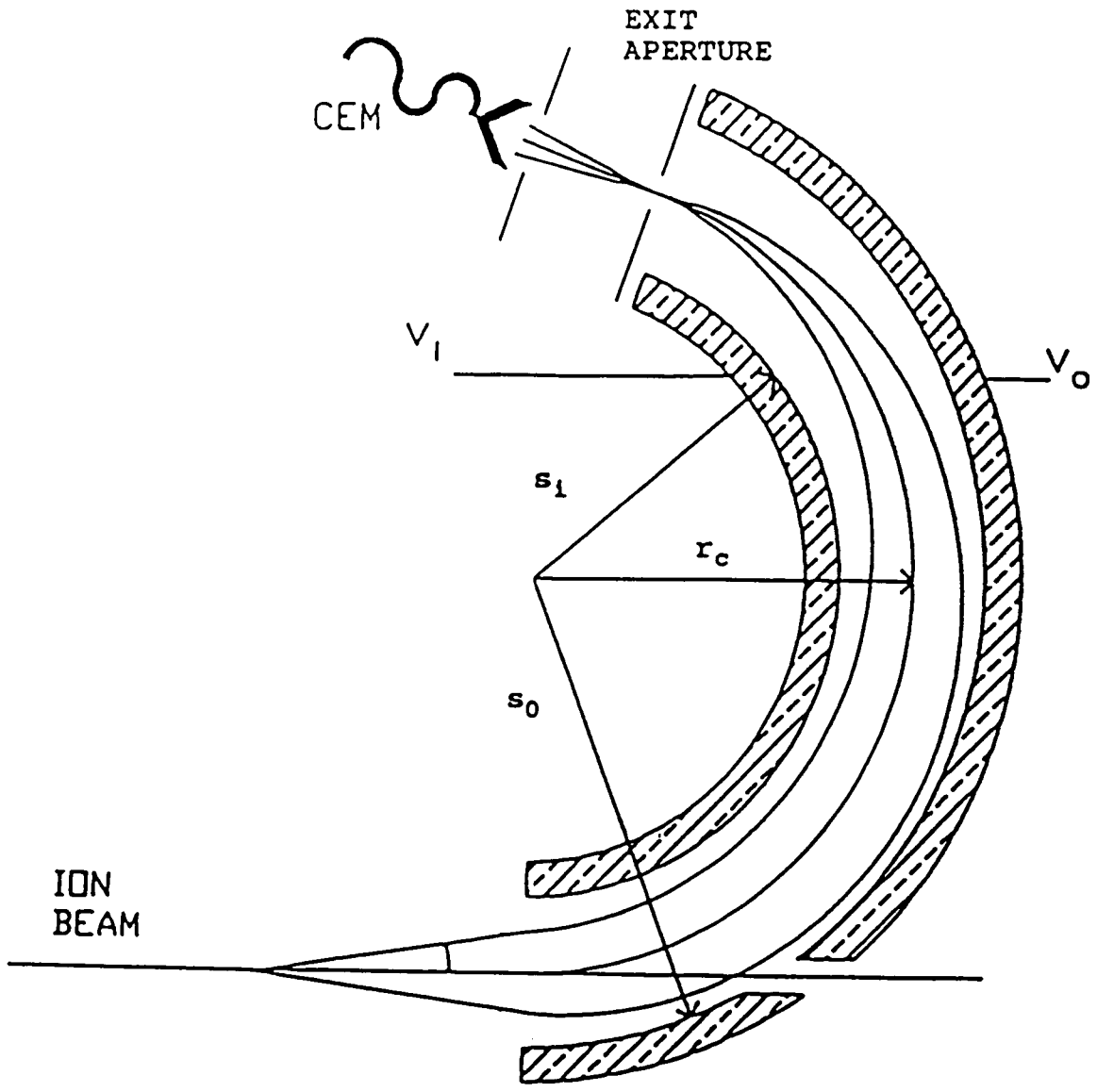

FIGURE 2.4 SCHEMATIC DIAGRAM OF THE 160^0 SPHERICAL SECTOR ANALYZER

direction of the central ray. The limiting values of these angles are $\pm\alpha_s$ and $\pm\beta_s$.

For electrons moving along the central ray the ratio of the potential difference ΔV across the two sectors to the electron kinetic energy T_c is a constant depending only on the geometry. The analyzer constant is defined as

$$C = e\Delta V / T_c. \qquad (2.11)$$

Given the field in the analyzer, (eq. 2.10), we can calculate T_c for a given ΔV. By inserting this into (eq. 2.11), we find

$$C = (s_o / s_i) - (s_i / s_o). \qquad (2.12)$$

Particles moving along the central ray of the analyzer enter the analyzer at

$$r_o = r_c = (s_o + s_i) / 2, \qquad (2.13)$$

midway between the spherical plates. The differential equation of the path of a charged particle entering at an arbitrary r_o with energy T is

$$\partial^2 u/\partial\theta^2 + u = r_c \cdot T_c/(r_o \cdot T \cdot \cos^2\alpha), \qquad (2.14)$$

where $u = r_o/r$ and θ is the total angle of deflection. Due to the spherical symmetry, the analyzer provides perfect focussing for the angle β. The solution of the differential equation (eq. 2.14) is

$$r_0 / r = (r_c \cdot T_c/(r_o \cdot T \cdot \cos^2\alpha)) \cdot (1 - \cos\theta) + \cos\theta - \tan\alpha \cdot \sin\theta. \qquad (2.15)$$

If we expand the factors containing α, and allow $\theta = 180^\circ$, then the last term vanishes and with it the only term that

is first order in α. So for $\theta = 180^{\circ}$ we will have first order focusing in the plane of deflection. Expanding (eq. 2.15), with $\theta = 180^{\circ}$, to second order in α yields

$$r_o / r_{180} = 2 \cdot (T_c \cdot r_c / T \cdot r_o) \cdot (1 + \alpha^2) - 1. \qquad (2.16)$$

A clear disadvantage of the 180° analyzer is that the object as well as the image point lies at the boundaries of the sector. Placing a detector at the image point can perturb the radial electric field at the sector boundaries. To avoid this problem in our experiment we use 160° sectors. The 160° analyzer preserves the properties of the 180° spherical sector analyzer to a good degree, while it adds the advantage that the object and image point are removed from the sector boundaries.

For our analyzer, whose dimensions are given in table 2.4, the sum of the distances of the image and object points from the sectors is 19.1 mm. Our analyzer does not have an entrance aperture, so the source size at the entrance determines the effective entrance aperture. The exit aperture is a slot 5.5 mm long and 1.5 mm wide, with the length perpendicular to the plane of deflection. The slot is used instead of a circular aperture so that a small misalignment of the analyzer does not prevent particle transmission and detection. The width of the slot and the source size determine the energy resolution of the analyzer. Particles transmitted through the exit aperture of the analyzer are detected by a CEM located 2.5 cm away. The

TABLE 2.4

DIMENSIONS AND PROPERTIES OF THE 160^0 SPHERICAL SECTOR ENERGY ANALYZER

Definition	Parameter
Inner sector radius	s_i = 4.9 cm
Outer sector radius	s_0 = 6.0 cm
Central ray	r_c = 5.45 cm
Angular acceptance	$\Phi = 6.8^0$
Energy resolution	$\Delta T/T$ = 1.4 %
Analyzer constant	$\Delta V/T$ = .43 V/eV

6 mm diameter aperture preceding the CEM determines the angular acceptance of the detector.

During the experiment we scan the voltages on the two sectors so that the central ray's potential stays constant. As we scan, the potential difference changes between the sectors. As the potential difference changes, electrons of different energies are deflected and transmitted through the analyzer. We do this to determine the energy distribution of Rydberg electrons that are field ionized and accelerated within the ionizer.

G. MODIFICATIONS

We used the apparatus, as it existed from previous experiments, to acquire preliminary data for our experiment. During these preliminary experiments the background pressure in the experimental chamber was on the order of $5 \cdot 10^{-6}$ torr. Two layers of μ metal shielding were used to reduce stray

magnetic fields near the apparatus. They lined the entire inside of the chamber, and therefore restricted pumping in the chamber. The resulting high background pressure in the chamber caused an increase in the background contributions in the spectra, and this increased uncertainties in our results.

The earlier shielding was composed of two large 3/16" thick μ metal cylinders. We have built a new shield composed of a single rectangular box of 1/32" μ metal. The surface area of the new shield is considerably less than the old shield allowing us to properly shield the apparatus while not blocking the valve to the diffusion pump. We have further modified the shield by inserting pump out holes in strategic places that allow maximum pumping while still shielding the apparatus. This new design allows us to reduce the pressure in the chamber to $2 \cdot 10^{-7}$ torr.

The alignment of the components which make up the apparatus must be done as precisely as possible. If there is any misalignment between the components of the apparatus electrons and ions scattered by the edges of the apertures will cause extensive background contributions in our spectra.

Previous to our experiment the alignment of the components was accomplished by establishing a reference line through the centers of the entrance and exit apertures of the 160^0 analyzer. The 160^0 analyzer was fixed to the

mounting plate of the apparatus and the reference line was determined by the use of a telescope. Then the spherical ionizer and the 30^0 analyzer, which were capable of vertical and horizontal translations, were aligned such that their entrance and exit apertures also were centered on the reference line. The two plates that make up the ionizer moved independently and the many degrees of freedom of movement of the ionizer made the alignment process tedious. It often seemed nearly impossible to guarantee proper alignment.

To eliminate alignment errors and make the alignment process easier we have machined a stand for the ionizer which does not move. The 160^0 analyzer mounts to the back plate of the ionizer and a solid mount holds both components. Our reference line is now determined by the apertures of the ionizer and the 160^0 analyzer.

In the past the 30^0 analyzer was aligned by positioning the analyzer by hand on the apparatus plate such that its entrance and exit apertures were centered on the reference line. To align the 30^0 analyzer to the other components we have built mechanical positioning adjusters that allow precision placement of the analyzer. The alignment process is now quicker and more precise, and the background contributions due to scattered electrons and ions have been reduced.

H. ELECTRONICS

The signals from the CEM and the multidynode detector are processed by front end NIM electronics as described below. The data acquisition is controlled by a LeCroy 3500 multichannel analyzer (MCA). The data are stored in histogramming memory by three multichannel scaling modules (MCS) and two analog to digital converters (ADC). The three MCS modules store the total number of stripped Rydberg electrons as a function of stripped Rydberg electron energy, the total number of stripped Rydberg electron-projectile ion coincidences as a function of the Rydberg electron energy, and the number of Rydberg electron-projectile ion random coincidences as a function of Rydberg electron energy. All three modules use 256 memory channels. Channel zero records the number of times the Rydberg electron energy is scanned over its range. Each of the remaining channels correspond to a particular energy band within the range.

I. SIGNAL DETECTION AND PROCESSING

Pulses from the CEM and the multidynode detectors are composed of real and noise signals. In order to eliminate contributions due to noise, the pulses are amplified by an Ortec 863 timing filter amplifier and input into a EG&G 8000 constant fraction discriminator. The discriminator level is set to determine the minimum voltage amplitude of pulses to be transmitted to its output. By observing the amplified

detector signal on an oscilloscope, the appropriate discriminator level for eliminating noise contributions is determined. The negative NIM output from the discriminator is converted to a positive TTL pulse in a LRS 688AL level adapter so that it can be counted by an MCS for electrons, or a counter/timer for ions.

The discriminated ion signal forms the input into an Ortec 776 counter/timer (CT). The CT counts for a preselected number of input signals. After the appropriate number of signals are counted, the CT outputs an end-of-cycle signal. The output signal serves two functions. First, it is delayed ~ 10 ns and used to trigger the CT in order to restart the counting sequence. Secondly, it forms the channel advance signal for the LeCroy MCS modules.

The Rydberg electron signals are counted in MCS modules with each channel corresponding to a Rydberg electron energy. Detected electrons are counted in each channel until the CT has counted the preselected number of ions. Once the CT's output signal is sent, the MCS's channel is advanced and counting begins for the next energy.

With each channel increment in the MCS, a digital channel address is available for external voltage programming of the analyzer power supply. The digital address is converted to an analog signal between zero and ten volts in a digital to analog converter (DAC). The magnitude of the analog signal is proportional to the

channel number.

For the voltage across the 160° spherical sector energy analyzer, three independent power supplies must be used, and each must be programmed. Both sectors of the analyzer must be raised to the high positive potential that is placed on the spherical ionizer. The analog DAC signal is fed into a pair of resistor chains to produce two voltages. The voltage for the inner sector of the analyzer is 55 percent of the DAC input signal. The voltage for the outer sector is 45 percent of the DAC signal. The modified DAC signal for each sector is input into separate summer invertors. The programming voltage for the spherical ionizer power supply is also input into the summer invertors. One of the summer invertors sets the programming voltage for the power supply of the inner sector by adding the two input voltages. The summer invertor feeding the power supply of the outer sector sets the programming voltage by subtracting the modified DAC signal from the ionizer programming voltage (see fig. 2.5).

J. COINCIDENCE PROCESSING

To determine how many Rydberg electrons accompany a particular projectile ion of exit core charge state q leaving the collision region, standard Rydberg electron-projectile ion coincidence measurements are made.

Electron signals that are processed and then output by

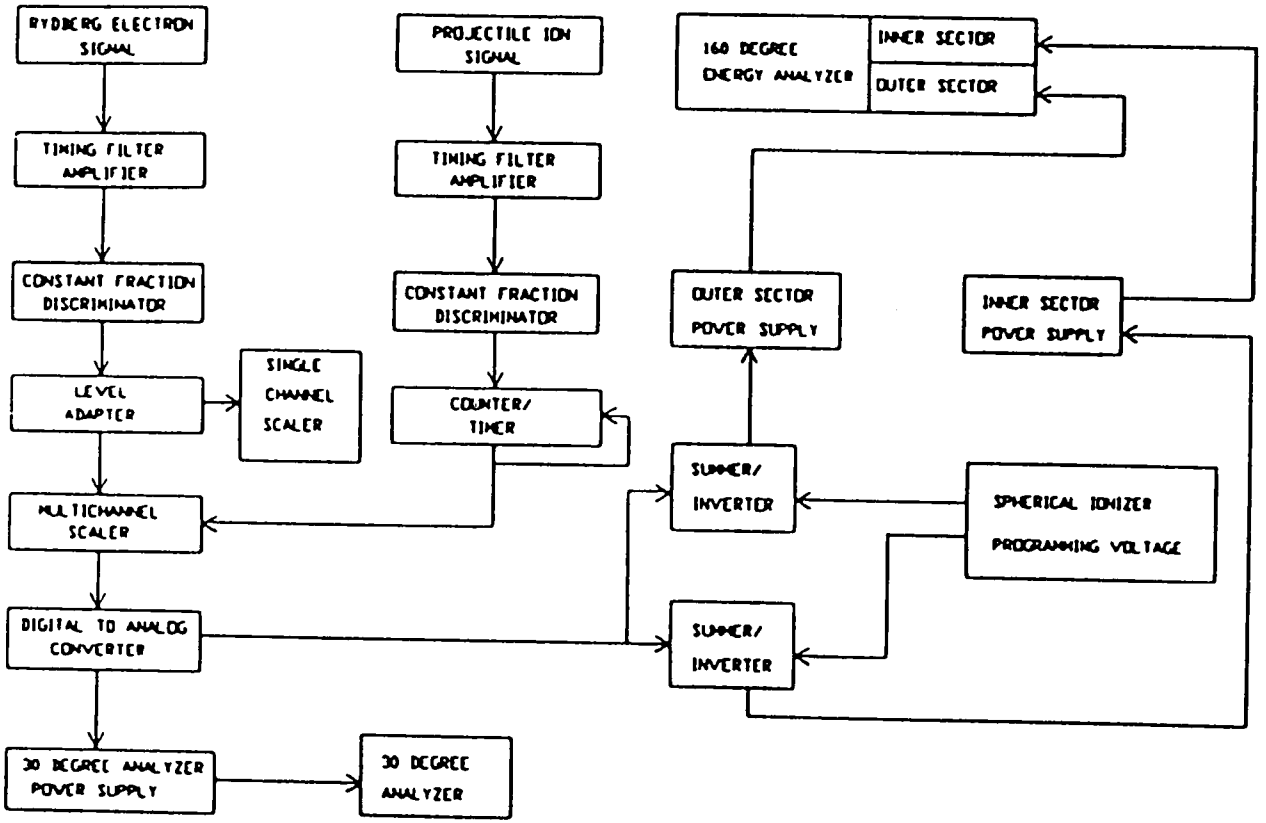

FIGURE 2.5 SCHEMATIC DIAGRAM OF ELECTRONICS USED TO DETECT RYDBERG ELECTRONS

the constant fraction discriminator form the start pulses of an Ortec 567 time-to-amplitude converter (TAC). The ion signals that are processed form the stop pulses of the TAC. The TAC produces a positive analog output pulse with an amplitude between zero and ten volts whose height is proportional to the difference in time Δt between the start and stop signals. The output pulse is fed into a ADC module which converts the signal amplitude into a digital signal which is proportional to Δt. The digital signal corresponds to the address of one of the 250 channels within the ADC module. The counts in this channel are incremented by one.

We find that the Rydberg electron-projectile ion coincidences appear as peaks in the ADC spectrum. A single channel analyzer (SCA) is used to choose only TAC pulses which correspond to the peak in the ADC spectrum. These pulses represent coincidences which are stored in the ADC in the time interval Δt. These coincidences are then counted as a function of the Rydberg electron energy in the MCS module (see fig. 2.6).

We use two SCA's to allow us to set two separate windows for viewing. One window is set to detect coincidences at the peak position. The second window is set to detect random coincidences away from the peak. By using two separate windows we are able to subtract the random coincidences from the total coincidences in the peak. This gives a straight forward method for determining real coincidences.

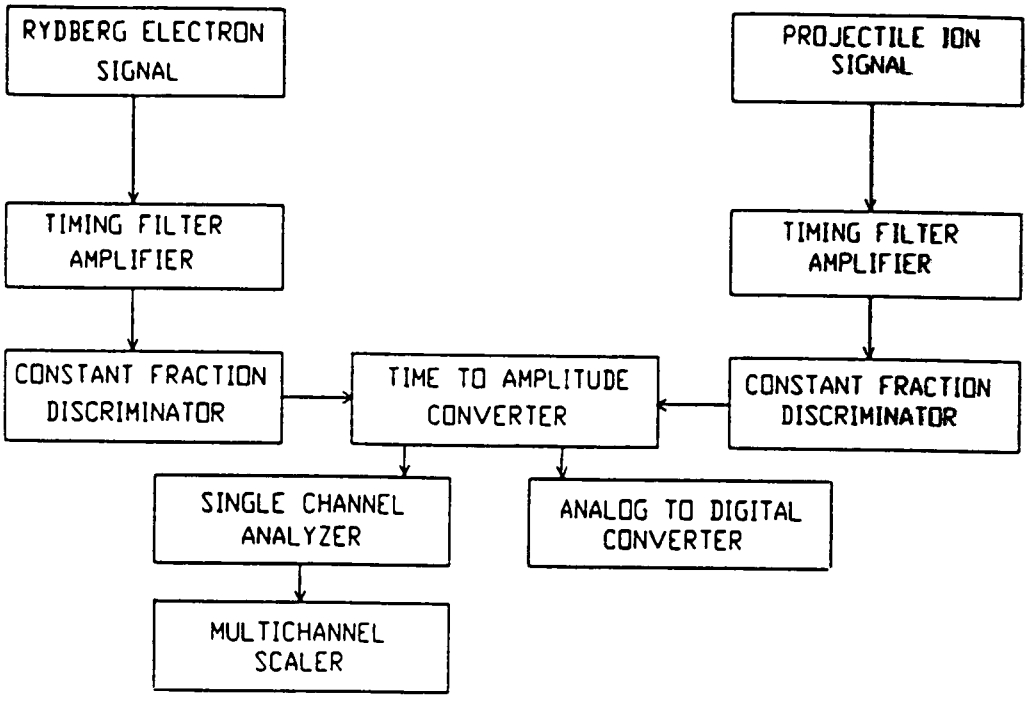

FIGURE 2.6 SCHEMATIC DIAGRAM OF ELECTRONICS USED TO MEASURE RYDBERG ELECTRON-PROJECTILE ION COINCIDENCES

CHAPTER 3

DATA ANALYSIS

The following types of measurements are made during our experiment. With 1000 V and then 500 V on the ionizer we record the total number of stripped Rydberg electrons, the total number of stripped Rydberg electron-projectile ion coincidence, and the total number of stripped Rydberg electron-projectile ion random coincidences for projectile ions of exit core charge states 3+, 4+, 5+, 6+, and 7+ as a function of the stripped Rydberg electron's kinetic energy. All of the measurements are repeated with gas cell pressures of 0 mtorr, 0.41 mtorr, 0.82 mtorr, and 1.23 mtorr, and are normalized to the total number of projectile ions of a selected exit core charge state which are detected.

Figure. 3.1a shows a typical spectrum of the total number of Rydberg electrons detected after being stripped in the ionizer for 0.1 MeV/u Ag^{4+} projectiles passing through an Ar gas target. The total number of stripped Rydberg electrons is plotted versus their kinetic energy in the laboratory frame. There are four primary regions of interest in this spectrum. The peak that appears at ≈ 1040 eV corresponds to Rydberg electrons that are stripped at the entrance to the spherical ionizer. Table 2.2 lists the principle quantum numbers, n_c, of the most tightly bound

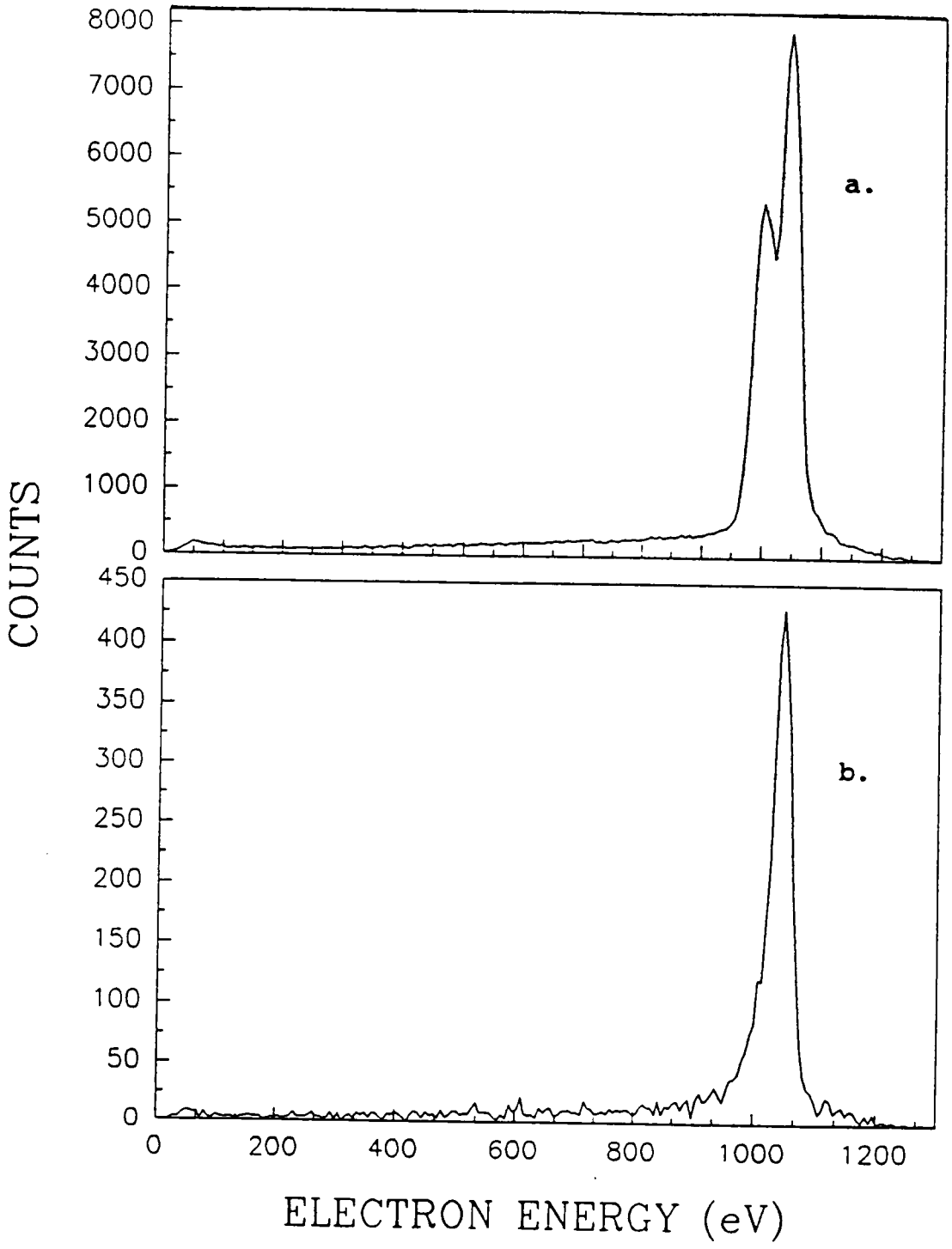

FIGURE 3.1 NUMBER OF RYDBERG ELECTRONS DETECTED VERSUS THEIR LABORATORY FRAME KINETIC ENERGY
a) TOTAL NUMBER OF RYDBERG ELECTRONS DETECTED
b) NUMBER OF RYDBERG ELECTRONS DETECTED IN COINCIDENCE WITH A PROJECTILE ION OF EXIT CORE CHARGE STATE 5+

electrons ionized at the entrance for each exit core charge state q, for each ionizer voltage. The peak that appears at ~ 1000 eV represents secondary electrons produced by scattered ions striking the spherical ionizer entrance aperture. These electrons leave the ionizer surface with ~ 0 eV and are accelerated through the ionizer. Upon exiting the ionizer these electrons have kinetic energy ~ 1000 eV.

The secondary and the Rydberg electron energy distributions overlap. To accurately determine the contribution from secondary and Rydberg electrons, each spectrum is analytically fit to a function consisting of the sum of two Gaussians

$$F(T) = a \cdot \exp(-b^2(c-T)^2) + d \cdot \exp(-e^2(f-T)^2), \qquad (3.1)$$

where a and d are the amplitudes of the Gaussians corresponding to the secondary and Rydberg electron distributions, respectively, and T is the kinetic energy of the Rydberg electrons. The energies of the peaks are given by c and f. The widths of the distributions are determined by b and e.

The third region, between ~ 250 eV and ~ 900 eV, is nearly featureless. This section of the spectrum corresponds to Rydberg electrons that are ionized by the electric field between the two sectors of the ionizer.

If we assume that the Rydberg states of the projectile ions are hydrogenic, then the energy of an electron in a Rydberg state of an ion is

$$E_n = -C/n^2, \tag{3.2}$$

where C is a constant, and n is the principal quantum number. From this relation we have

$$E_{n+1} - E_n = \Delta E_n / \Delta n = -(C/(n+1)^2) + C/n^2, \tag{3.3}$$

which for large n yields

$$\Delta E_n/\Delta n \approx 2C/n^3. \tag{3.4}$$

So the number of n-states in an energy interval ΔE_n is proportional to n^3. If we assume that the probability for excitation or capture to an n-state is proportional to $1/n^3$, then the number of electrons found in each energy interval with the same width ΔE_n is constant[5].

The lowest n-states n_c that will be ionized by an electric field of strength F, is proportional to $1/F^{1/4}$. If the electric field is proportional to $1/r^2$, then n_c is proportional $\sqrt{r}$. So the energy of the most tightly bound atomic electron ionized by F(r) is

$$E_{nc} = -C/n_c^2 = -B/r, \tag{3.5}$$

and

$$\partial E_{nc}/\partial r = B/r^2, \tag{3.6}$$

where B is a constant of proportionality.

The number of electrons ionized in an interval between r and r + Δr is proportional to the width of the energy interval between r + Δr. If the number of excited electrons per unit energy interval is constant, then the number of electrons ionized between r and r + Δr is proportional to $\Delta r \cdot B/r^2$.

In our experiment we use a spherical sector ionizer to strip electrons in high n-states of the ion. The electric field in the ionizer is given by

$$F(r) = [V_i \cdot r_i \cdot r_o/(r_o - r_i) \cdot r^2]. \quad (3.7)$$

the potential inside the ionizer is

$$V(r) = [V_i \cdot r_i \cdot r_o/(r_i - r_o)] \cdot (1/r_o - 1/r). \quad (3.8)$$

An electron that is ionized at a position r inside the field will exit the ionizer with kinetic energy T, where

$$T = (1 - r_i/r) \cdot [e \cdot V_i \cdot r_o/(r_o - r_i)] + 54.4 \text{ eV} \quad (3.9)$$

and

$$\partial T/\partial r = [e \cdot V_i \cdot r_o/(r_o - r_i)] \cdot r_i/r^2. \quad (3.10)$$

Electrons with kinetic energy $T \pm \Delta T$ that are ionized in the ionizer, in an interval

$$\Delta r = [(r_o - r_i)/e \cdot V_i \cdot r_o \cdot r_i] \cdot r^2 \Delta T \quad (3.11)$$

will be passed by the 160^0 analyzer when the analyzer is tuned to T. If ΔT is proportional to T, $\Delta T = \lambda T$, then the number of electrons observed in the featureless region, when the analyzer is tuned to T is given by

$$\Delta r \cdot B/r^2 = B \cdot \lambda T \cdot (r_o - r_i)/e \cdot V_i \cdot r_o \cdot r_i, \quad (3.12)$$

i.e. the number of electrons with kinetic energy T is proportional to T. The electrons that are in the spectra of the total number of stripped Rydberg electrons show such a T dependence does exist in the featureless regions. Table 3.1 lists the range of the principle quantum number n for Rydberg electrons detected with T for different exit core charge states of the projectile ion at each ionizer voltage.

TABLE 3.1

N-LEVELS USED IN DETERMINING THE PRODUCTION PROBABILITIES FOR RYDBERG ELECTRONS STRIPPED IN THE SPHERICAL SECTOR IONIZER, WITH 500 V AND 1000 V ACROSS THE IONIZER

q	$n(F_1)$	$n(F_2)$
a. 500 V.	250 eV	400 eV
3	83	81
4	103	100
5	122	119
6	140	136
7	157	153
b. 1000 V.	315 eV	900 eV
3	70	67
4	87	83
5	103	99
6	118	113
7	133	127

The presence of the small peak at ~ 54 eV, in (fig. 3.1a) is at the moment not completely understood, but is probably due to cusp electrons produced by ions colliding with background gas atoms in the region between the ionizer exit and the entrance to the 160^0 analyzer.

To obtain the real Rydberg electron-projectile ion coincidence spectrum we subtract the random coincidences from the total coincidences. All spectra have a similar structure but the peak corresponding to the secondary electrons is reduced considerably in the real coincidences spectrum (see fig. 3.1b). This occurs because the scattered

ions that dislodge secondary electrons have a very slim chance of reaching the detector.

To determine the probability that an incident Ag^{4+} ion produces a Rydberg electron, and a Rydberg electron in coincidence with a Ag^{q+} ion we must normalize the number of Rydberg electrons and the number of stripped Rydberg electron-projectile ion coincidences detected to the total number of projectile ions passing through the target region. Since during the experiment we are only detecting projectile ions of a selected exit core charge state q, it is necessary to determine the charge state fractions and the detection efficiency of the multidynode detector to find the total number of silver ions passing through the apparatus.

A. CHARGE STATE FRACTIONS

During the experiment the total number of Rydberg electrons stripped by the electric field in the ionizer, and the total number of Rydberg electron-projectile ion coincidences are measured. They are then normalized to the total number of ions of a given exit core charge state. Measurements are made at four different gas pressures. To determine the production cross sections from these measurements, the total number of ions passing through the gas cell and the absolute pressure in the gas cell need to be known. Both can be determined after the exit charge state fractions have been calculated.

We define the exit charge state fraction as f(q,p) at a given gas pressure as

$$f(q,p) = \frac{\text{number of ions of exit charge state } q+}{\text{total number of incident ions}} . \quad (3.13)$$

To determine the charge state fractions we assume that the total number of Rydberg electrons stripped by the electric field in the ionizer at a given gas pressure is proportional to the total number of projectile ions passing through the gas cell. If we define

$$f'(q,p) = \frac{\text{number of ions of exit charge state } q+}{\text{total number of Rydberg electrons}} , \quad (3.14)$$

then we have

$$b \cdot f'(q,p) = f(q,p), \quad (3.15)$$

i.e. f'(q,p) is proportional to f(q,p).

The first step in calculating the charge state fractions is to determine f'(q,p) for each charge state at each gas pressure. Then, we sum the value f'(q,p) for all charge states at each pressure, such that

$$\Sigma f'(q,p) = c. \quad (3.16)$$

If we let b = 1/c, then our charge state fractions will be normalized to one:

$$b \cdot \Sigma f'(q,p) = \Sigma f(q,p) = 1. \quad (3.17)$$

Our measurements directly yield f'(q,p) and therefore, after determining b, the charge state fractions f(q,p) are known.

We find that the fraction of ions exiting the target area with the incident charge state q=4 is greater than 90 percent, because our measurements are made under single

collision conditions, and the probability that an ion of charge state q=4 changes its charge to exit charge state q is small. By normalizing the sum of all charge state fractions to one, we couple the charge state fractions so that a small error in the calculation of the q=4 exit charge state fraction may introduce large errors in the charge state fractions for q≠4. To avoid this possibility we have employed a second method of calculating the charge state fractions that does not couple the charge state fractions, but rather determines each charge state fraction independently.

We measure the total number of Rydberg electrons stripped by the electric field in the ionizer normalized to the total amount of charge collected in a Faraday cup. From the charge collected in the Faraday cup we determine the total number of incident projectile ions. If we define

$$f''(q,p) = \frac{\text{number of incident projectile ions}}{\text{total number of Rydberg electrons}} \qquad (3.18)$$

then we have

$$f(q,p) = f'(q,p) \;/\; f''(q,p). \qquad (3.19)$$

In this method, it is assumed that the detection efficiency of the Faraday cup and the single ion detector are equal. While the detection efficiency of the Faraday cup is assumed to be one, the detection efficiency of the single ion detector is known to be less than one. Only after the detection efficiency of the single ion detector has been determined, do we obtain absolute charge state

fractions. And still this method will allow $\Sigma f(q,p) \neq 1$, due to the errors introduced in the detection efficiency.

Both methods give consistent results for all charge state fractions calculated. Under single collision conditions the charge state fractions are linear with target gas pressure. To determine the most accurate values for the charge state fractions we have fit the average of both methods versus gas pressure. Through out the remainder of the analysis we use the fitted values for the charge state fractions (see table 3.2).

Under single collision conditions the probability that an ion of incident charge state q=4 changes its charge to exit charge state q is proportional to the target gas pressure. During the experiment we only know the relative pressure p' in the gas cell. We therefore write

$$\text{Prob.}(4\rightarrow q,p') = n'_0 \cdot \sigma(4\rightarrow q) \cdot \ell \cdot p' \qquad (3.20)$$

where n'_0 is the number of target atoms per unit volume (cm^3) per unit relative gas pressure (p'), $\sigma(4\rightarrow q)$ is the charge exchange cross section for the incident charge state 4 changing to exit charge state q, and ℓ is the effective gas cell length.

The charge state fractions as a function of the target gas pressure are given by

$$f(q,p') = f(q,0) + \text{Prob.}(4\rightarrow q,p'), \qquad (3.21)$$

where

$$\text{Prob.}(4\rightarrow q,p') = a \cdot p'. \qquad (3.22)$$

TABLE 3.2

FITTED CHARGE STATE FRACTIONS

q+	P(mtorr)	f(q,p)
3	0.0	.0037
3	0.41	.0144
3	0.82	.0251
3	1.23	.0361
4	0.0	.9925
4	0.41	.9747
4	0.82	.9568
4	1.23	.9386
5	0.0	.0017
5	0.41	.0056
5	0.82	.0095
5	1.23	.0136
6	0.0	.0008
6	0.41	.0030
6	0.82	.0052
6	1.23	.0075
7	0.0	.0007
7	0.41	.0019
7	0.82	.0032
7	1.23	.0045

We determine Prob.(4→q,p) from linear fits of the average charge state fraction f(q,p'), determined from the two previous methods, versus the relative target gas pressure p'. The fits are of the form

$$f(q,p') = a \cdot p' + b \qquad (3.23)$$

and, from (eq. 3.22), yield

$$\text{Prob.}(4\rightarrow q,p'=1) = a. \qquad (3.24)$$

As stated above, during the experiment we only know the relative pressures p' in the gas cell. In order to find the absolute pressure in the gas cell, we will rewrite (eq. 3.20)

$$\text{Prob.}(4\rightarrow q,p) = n_0 \cdot \sigma(4\rightarrow q) \cdot \ell \cdot p(\text{mtorr}). \qquad (3.25)$$

Now, p is the absolute pressure in the gas cell in mtorr, and n_0 is the number of target atoms per cm^3 per mtorr and from the ideal gas law it is calculated to be $3.535 \cdot 10^{13}$ cm^{-3}. The charge exchange cross sections $\sigma(4\rightarrow 3)$, $\sigma(4\rightarrow 5)$, and $\sigma(4\rightarrow 6)$ are known from a previous experiment,[12] and we have just determined Prob.(4→q,p). We now can determine the absolute gas cell pressures used in our measurements from (eq. 3.25). After having determined the absolute pressure we can solve (eq. 3.25) for the charge exchange cross section $\sigma(4\rightarrow 7)$.

B. ION DETECTION EFFICIENCY

All of the ions exiting the target region with a selected core charge state q are not detected by the multi-

dynode electron multiplier. The fraction of projectile ions that is detected is equal to the detection efficiency ϵ_i. We know that each Rydberg electron detected by the CEM must have been associated with an ion that left the collision region with some core charge state q. If we denote the number of Rydberg electrons detected in coincidence with a projectile ion of charge state q as Ryd(q) and we denote the total number of Rydberg electrons detected, normalized to the same number of incident ions, as Ryd, then the detection efficiency is

$$\epsilon_i = \sum_{q=3}^{7} \mathrm{Ryd}(q) \; / \; \mathrm{Ryd} \qquad (3.26)$$

For a detector that is 100 percent efficient ϵ_i is equal to one. In our experiment the detection efficiency is determined to be 21.5 ± 0.5 percent from (eq. 3.26).

C. PRODUCTION PROBABILITIES

After being stripped from the ion by the electric field in the ionizer, electrons that are emitted into a cone of solid angle $\Delta\Omega$ are detected. $\Delta\Omega$ is centered on the beam direction and is determined by the diameter of the entrance aperture of the CEM and its distance from the exit aperture of the analyzer. The energy distribution of the detected electrons in the laboratory frame is measured as the voltage across the sectors of the 160^0 spherical sector analyzer is scanned. The number of Rydberg electrons N_i having a

laboratory frame energy in the interval $T_i \pm \Delta T/2$ is counted for each voltage V_i across the 160^0.

We want to determine the probability that a projectile electron in a state with principle quantum number n_i between n and $n + \Delta n$ is produced in a collision between the projectile ion and a gas atom. Rydberg electrons with a given quantum number n are stripped at a well defined radius r in the ionizer and therefore exit the ionizer with a well defined kinetic energy T (see eq. 3.9). The measured number of stripped Rydberg electrons N_i, with kinetic energy between $T \pm \Delta T$ is related to the production probability through

$$N_i = N_p \cdot \int_{\Delta\Omega} \int_{\Delta T} P(T,\Omega) \cdot e_{160}(T)\ dT\ d\Omega, \qquad (3.27)$$

where N_p is the total number of Ag^{4+} projectile ions incident during the time interval when the analyzer voltage is V_i, $P(T,\Omega)$ is the probability of producing an electron in a Rydberg state of the projectile ion with kinetic energy T after being stripped from the ion, and $e_{160}(T)$ is the 160^0 analyzer transmission/detection efficiency.

The 160^0 analyzer transmission/detection efficiency is a product of the analyzer's transmission function and the electron detection efficiency of the CEM. The transmission function is determined by the width of the electron beam as it enters the 160^0 analyzer, and by the exit aperture of the 160^0 analyzer. In order to determine the transmission /detection efficiency we must understand the focusing

properties of the ionizer.

The electric field between the spherical sectors of an ideal spherical ionizer is proportional to $1/r^2$ and zero everywhere else. If a projectile ion enters the region between the sectors through an aperture in the outer sector it will feel the electric field immediately. As the ion exits the region through an aperture in the inner sector the field abruptly goes to zero.

The electric field of a real ionizer is characterized by fringe fields near the entrance and exit apertures as well as near the sector boundaries. The fringe fields near the entrance and exit aperture alter the focusing properties of the ionizer and cause the kinetic energy of electrons that are stripped at the entrance and exit of the ionizer to be detected with slightly lower energy than expected.

We have modelled the electric field between the sectors of our ionizer using a ray tracing program. Using this model we have investigated the focusing properties of the ionizer. Figure 3.2 shows a typical set of simulated electron trajectories passing through the ionizer, with the equipotential lines near the entrance and exit apertures also shown.

We find that due to the focusing properties of our ionizer, the size of the stripped Rydberg electron beam entering the 160^0 analyzer is different for different ionizer voltages. As a consequence of this, the

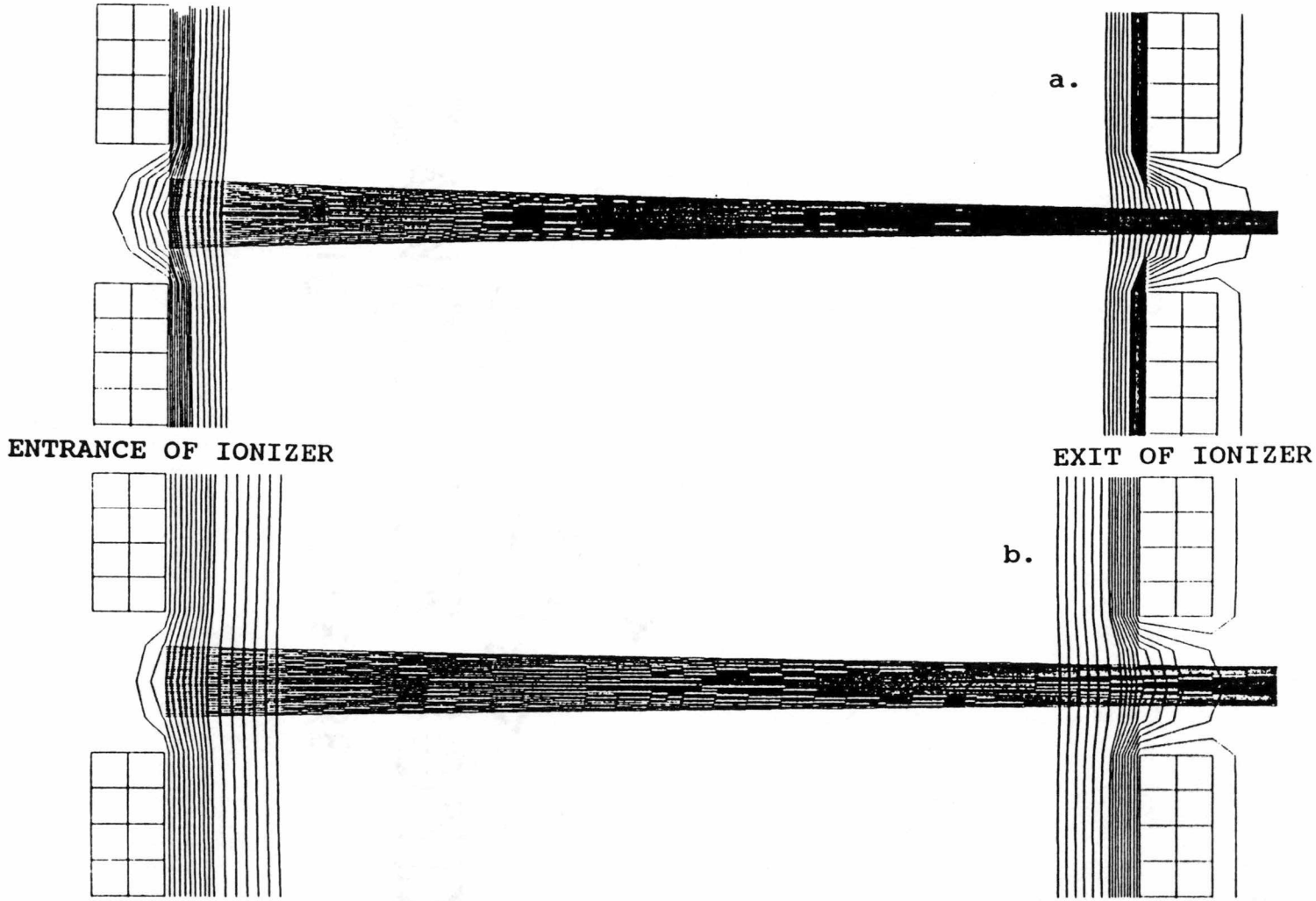

FIGURE 3.2 MODELLED ELECTRON TRAJECTORIES FOR A 2 mm BEAM COMPOSED OF 54.4 eV ELECTRONS WITH a) 1000 V AND b) 500 V ACROSS THE IONIZER

transmission function of the 160^0 analyzer is different for each ionizer voltage.

We have modelled the transmission/detection efficiency of the 160^0 analyzer and found it to be independent of the solid angle $\Delta\Omega$ for small $\Delta\Omega$ about the beam direction. If we assume that it is non-zero only over a small energy interval, and that the probability $P(T,\Omega)$ varies slowly over this energy interval, we can take the $P(T,\Omega)$ out of the energy integral, and rewrite (eq. 3.27) as

$$N_i = N_p \cdot \int_{\Delta\Omega} P(t,\Omega)\ d\Omega \int_{\Delta T} e_{160}(T)\ dT. \qquad (3.28)$$

From a computer model we have developed it is determined that $e_{160}(T)$ is approximately trapezoidal in shape so that

$$\int_{\Delta T} e_{160}(T)\ dT = e_{160}(T_i) \cdot \Delta T_i, \qquad (3.29)$$

where ΔT_i is the full width at half maximum (FWHM) of $e_{160}(T_i)$. For given entrance and exit apertures of the 160^0 analyzer $\Delta T/T = \lambda$ = constant, and $\Delta T = \lambda T$. Now inserting (eq. 3.29), into (eq. 3.28) we obtain

$$\int_{\Delta\Omega} P(T,\Omega)\ d\Omega = N_i \ / \ (N_p \cdot e_{160}(T_i) \cdot \lambda T_i). \qquad (3.30)$$

To obtain the probability for producing a stripped Rydberg electron with laboratory frame energy in an energy range between T_i to T_f we integrate the probability function over the energy interval

$$\int_{T_i}^{T_f} \int_{\Delta\Omega} P(T,\Omega)\ d\Omega\ dT \simeq \sum_i^f N_i \cdot \delta T_i \ / \ (N_p \cdot e_{160}(T_i) \cdot \lambda T_i), \qquad (3.31)$$

where δT_i is the effective kinetic energy interval corresponding to a one channel increment in the Rydberg

electron spectrum. In our experiment δT_i is equal to 6.33 eV/channel and 3.17 eV/channel for the 1000 V data and the 500 V data, respectively.

In this experiment we have determined the probability that a projectile Rydberg electron in a state with principal quantum number n is produced in a collision of a projectile ion and a gas atom. We have determined the probabilities for producing Rydberg electrons in these collisions which are stripped at the entrance of the ionizer and in an interval Δr deeper in the ionizer, for each charge state at each ionizer voltage.

Once the probabilities are determined the Rydberg electron production cross sections are calculated from

$$\int_{T_i}^{T_f}\int_{\Delta\Omega} P(T,\Omega)\ d\Omega\ dT = n_0 \cdot \sigma(q+) \cdot \ell \cdot p \qquad (3.32)$$

as detailed in section 3A.

D. UNCERTAINTIES

Absolute uncertainties are uncertainties that effect all of the cross section calculations in the same way. In this experiment they arise from the uncertainties in the estimation of the effective gas cell length (ℓ), the uncertainties in the factor that relates the pressure in the feed tube to the pressure in the gas cell, and the uncertainties in the value used for the Rydberg electron detection efficiency. We assume that the method used to

determine ℓ has an inherent uncertainties of approximately 20 percent[12]. In all our results we set the absolute electron detection efficiency of the CEM's equal to one. From published values for different CEM we estimate a 30 percent uncertainties in this value. Our largest absolute uncertainties comes from the uncertainties in the transmission function of the ionizer and 160^0 analyzer combination, even though the focusing properties of the ionizer have been modelled. We therefore estimate the absolute uncertainties in the cross sections to be on the order of a factor of two.

Relative uncertainties do not effect all of the cross sections in the same way. Some of the sources of these uncertainties are statistical uncertainties, variations in the target gas pressure, and uncertainties in the calculated charge state fractions. The gas pressure in the tube that feeds the gas cell varied between five percent and fifteen percent during each experimental run at different gas pressures. This changing pressure could not be controlled due to the lag time of the flow rate controller.

Statistical uncertainties in the charge state fractions are relatively small. Due to uncertainties in the gas pressure, we determine the uncertainties in the charge state fractions f(q,p) from the fitting procedure giving the best straight line fit of charge state fraction versus gas pressure. The uncertainties in f(q,p) is determined from

the uncertainties in the slope of the linear fit.

Uncertainties in the probabilities for producing a Rydberg electron in coincidence with a projectile ion of core charge state q, $P(T,\Omega)$, are found from linear fits of $P(T,\Omega)$ versus gas pressure. The uncertainties in these fits are used to determine the relative uncertainties in calculating the production cross sections. When calculating cross sections and cross section ratios, uncertainties are quadratically propagated.

CHAPTER 4

RESULTS AND CONCLUSIONS

As stated in chapter one, the goal of our experiment is to measure the production cross sections for electrons in high Rydberg states of the projectile which fall into specified energy intervals. We examine the production cross sections for single and double target electron capture events, and single projectile electron excitation and projectile electron excitation plus ionization events for 0.1 MeV/u Ag^{4+} ions colliding with an Ar gas target. We then can determine if the n-state distribution of high Rydberg states that are populated in ion-atom collisions depends on the production process, i.e. if the n-state distribution is different for capture and excitation events or for one-electron and two-electron events.

To achieve our goal we have determined the production probabilities for Rydberg electrons in coincidence with the exit core charge states, 3+, 4+, 5+, 6+, and 7+ of the projectile ion. We have measured these production probabilities for Rydberg electrons which are stripped at the entrance of the ionizer and Rydberg electrons that are stripped from a pre-determined region inside the ionizer with 1000 V and then 500 V across the ionizer. From these probabilities we have calculated the corresponding

production cross sections.

A. CHARGE EXCHANGE CROSS SECTIONS

In table 4.1 we list the charge exchange cross sections which are determined from the fit of the exit charge state fractions of the projectile ion versus target gas pressure. Here $\sigma(4\rightarrow6)$ is the projectile electron excitation plus ionization cross section, $\sigma(4\rightarrow5)$ is the projectile ion single ionization cross section, and $\sigma(4\rightarrow3)$ is the cross section for single target electron capture plus capture to a lower lying bound state. The most probable interaction which causes the projectile to change charge is single target-electron capture followed by single projectile-electron loss and double electron loss, respectively.

B. RYDBERG ELECTRON PRODUCTION CROSS SECTIONS

The cross sections for the production of electrons in high Rydberg states of the projectile ions for which the principal quantum numbers n lie in a specified range are given in tables 4.2 and 4.3 for all selected exit core charge states. The ranges of the principal quantum number, n, in table 4.3 correspond to the range of kinetic energies of the stripped Rydberg electrons over which we have integrated the featureless part of our Rydberg electron spectra. Tables 4.4 and 4.5 list the same cross sections normalized per unit energy interval, i.e. divided by the

TABLE 4.1

PROJECTILE CHARGE EXCHANGE CROSS SECTIONS

$\sigma(4\rightarrow q)$	(10^{-16} cm^2)
$\sigma(4\rightarrow 3)$	5.1 ± 0.4
$\sigma(4\rightarrow 5)$	2.4 ± 0.2
$\sigma(4\rightarrow 6)$	1.13 ± 0.03
$\sigma(4\rightarrow 7)$	0.69 ± 0.04

TABLE 4.2

PRODUCTION CROSS SECTIONS (cm^2) FOR ELECTRONS STRIPPED AT THE ENTRANCE OF THE IONIZER, $n_{30} \geq n \geq n_c$

q	n_c	$\sigma(q+)$	$\Delta\sigma(q+)$
a. 500 V			
3	85	$2.0 \cdot 10^{-19}$	$1.9 \cdot 10^{-20}$
4	106	$1.3 \cdot 10^{-18}$	$2.4 \cdot 10^{-19}$
5	125	$7.2 \cdot 10^{-19}$	$7.8 \cdot 10^{-20}$
6	143	$4.8 \cdot 10^{-19}$	$2.0 \cdot 10^{-20}$
7	160	$4.1 \cdot 10^{-19}$	$2.0 \cdot 10^{-20}$
b. 1000 V			
3	71	$3.8 \cdot 10^{-19}$	$6.4 \cdot 10^{-20}$
4	88	$2.2 \cdot 10^{-18}$	$8.1 \cdot 10^{-20}$
5	105	$1.3 \cdot 10^{-18}$	$9.3 \cdot 10^{-21}$
6	120	$9.8 \cdot 10^{-19}$	$1.9 \cdot 10^{-20}$
7	135	$7.0 \cdot 10^{-19}$	$2.1 \cdot 10^{-20}$

TABLE 4.3

PRODUCTION CROSS SECTIONS (cm^2) FOR ELECTRONS IONIZED BY THE FIELD INSIDE THE IONIZER $n_1(F_1) \geq n \geq n_2(F_2)$

	q	(n_1, n_2)	$\sigma(q+)$	$\Delta\sigma(q+)$
a. 500 V		400 eV,250 eV		
	3	81,83	$3.7 \cdot 10^{-20}$	$1.2 \cdot 10^{-20}$
	4	100,103	$2.1 \cdot 10^{-19}$	$1.4 \cdot 10^{-20}$
	5	119,122	$7.4 \cdot 20^{-20}$	$9.9 \cdot 10^{-21}$
	6	136,140	$6.6 \cdot 10^{-20}$	$9.0 \cdot 10^{-21}$
	7	153,157	$4.6 \cdot 10^{-20}$	$6.0 \cdot 10^{-21}$
b. 1000 V		900 eV,315 eV		
	3	67,70	$6.7 \cdot 10^{-20}$	$6.4 \cdot 10^{-21}$
	4	83,87	$4.1 \cdot 10^{-19}$	$4.1 \cdot 10^{-20}$
	5	99,103	$1.5 \cdot 10^{-19}$	$8.5 \cdot 10^{-21}$
	6	113,118	$1.1 \cdot 10^{-19}$	$2.8 \cdot 10^{-21}$
	7	127,133	$9.2 \cdot 10^{-20}$	$8.0 \cdot 10^{-22}$

TABLE 4.4

PRODUCTION CROSS SECTIONS (cm^2) NORMALIZED PER UNIT ENERGY INTERVAL (eV) FOR ELECTRONS WITH $n_{30} \geq n \geq n_c$

	q	$\sigma(q+)$	$\Delta\sigma(q+)$
a. 500 V			
	3	$1.4 \cdot 10^{-17}$	$1.3 \cdot 10^{-18}$
	4	$7.9 \cdot 10^{-17}$	$1.4 \cdot 10^{-17}$
	5	$4.0 \cdot 10^{-17}$	$4.3 \cdot 10^{-18}$
	6	$2.4 \cdot 10^{-17}$	$9.8 \cdot 10^{-19}$
	7	$1.9 \cdot 10^{-17}$	$9.4 \cdot 10^{-19}$
b. 1000 V			
	3	$1.8 \cdot 10^{-17}$	$3.0 \cdot 10^{-18}$
	4	$8.9 \cdot 10^{-17}$	$3.3 \cdot 10^{-17}$
	5	$4.9 \cdot 10^{-17}$	$3.4 \cdot 10^{-18}$
	6	$3.3 \cdot 10^{-17}$	$6.3 \cdot 10^{-19}$
	7	$2.1 \cdot 10^{-17}$	$6.5 \cdot 10^{-19}$

TABLE 4.5

PRODUCTION CROSS SECTIONS (cm^2) NORMALIZED PER UNIT ENERGY INTERVAL (eV) FOR ELECTRONS WITH $n_1 \geq n \geq n_2$

q	$\sigma(q+)$	$\Delta\sigma(q+)$
a. 500 V		
3	$2.5 \cdot 10^{-17}$	$8.2 \cdot 10^{-18}$
4	$1.2 \cdot 10^{-16}$	$8.3 \cdot 10^{-18}$
5	$3.9 \cdot 10^{-17}$	$5.2 \cdot 10^{-18}$
6	$3.1 \cdot 10^{-17}$	$4.3 \cdot 10^{-18}$
7	$2.0 \cdot 10^{-17}$	$2.6 \cdot 10^{-18}$
b. 1000 V		
3	$2.9 \cdot 10^{-17}$	$2.8 \cdot 10^{-18}$
4	$1.5 \cdot 10^{-16}$	$1.5 \cdot 10^{-17}$
5	$5.2 \cdot 10^{-17}$	$2.8 \cdot 10^{-18}$
6	$3.6 \cdot 10^{-17}$	$8.6 \cdot 10^{-19}$
7	$2.6 \cdot 10^{-17}$	$2.3 \cdot 10^{-19}$

energy intervals that correspond to the range of n-states that Rydberg electrons are detected from for each projectile ion charge state. In both tables single electron capture to a high Rydberg state is most probable followed in importance by single excitation to a high Rydberg state, excitation plus ionization, and capture to a high Rydberg state plus capture to a lower lying bound state, respectively. We have only listed the relative uncertainties ($\Delta\sigma(q+)$), in these tables. Absolute uncertainties, which are on the order of a factor of two, do not affect cross section ratios given in the following tables.

In tables 4.6 and 4.7 we list the ratios of the

TABLE 4.6

RATIOS OF $\sigma(q+)_{1000}/\sigma(q+)_{500}$ NORMALIZED PER UNIT ENERGY INTERVAL FOR ELECTRONS STRIPPED AT THE ENTRANCE OF THE IONIZER $n_{30} \geq n \geq n_c$

q+	$\sigma(q+)_{1000}/\sigma(q+)_{500}$
3	1.24 ± 0.24
4	1.12 ± 0.21
5	1.22 ± 0.13
6	1.35 ± 0.06
7	1.15 ± 0.07

TABLE 4.7

RATIOS OF $\sigma(q+)_{1000}/\sigma(q+)_{500}$ NORMALIZED PER UNIT ENERGY INTERVAL FOR ELECTRONS STRIPPED INSIDE THE IONIZER $n_1 \geq n \geq n_2$

q+	$\sigma(q+)_{1000}/\sigma(q+)_{500}$
3	1.18 ± 0.41
4	1.23 ± 0.15
5	1.32 ± 0.19
6	1.14 ± 0.16
7	1.31 ± 0.17

production cross sections per unit energy interval obtained from the number of Rydberg electrons stripped at the entrance of the ionizer, and from the number of Rydberg electrons stripped inside the ionizer with 1000 V and 500 V across the ionizer, respectively. We find the ratios to be constant within error.

The cross sections for the excitation or capture of a target electron to a projectile ion Rydberg state with high principal quantum number n scale like n^{-3} in the first Born approximation[26]. Since this scaling factor exactly cancels the density of states which varies as n^3, electron capture and excitation cross sections per unit energy interval are assumed to be very slowly varying functions of the energy E_n of the final state. The function $\partial\sigma(E_n)/\partial E$ will approach the ionization limit with zero slope. We therefore expect the cross sections per unit energy interval for target electron capture to high Rydberg states and projectile electron excitation to high Rydberg states to be independent of the energy, E_n, and the energy range over which they are integrated.

The ratios in table 4.6 and 4.7 are then expected to be equal to one. We find the ratios to be close to one, differing from one by a small amount which we assume is mostly due to errors in the calculated transmission function.

In table 4.8 we list the production cross section

TABLE 4.8

RATIO OF PRODUCTION CROSS SECTIONS FOR RYDBERG ELECTRONS STRIPPED AT THE ENTRANCE TO THE IONIZER COMPARED TO RYDBERG ELECTRONS STRIPPED INSIDE THE IONIZER

	q	ratio
a. 500 V		
	3	5.54 ± 1.91
	4	6.25 ± 1.22
	5	9.67 ± 1.66
	6	7.34 ± 1.05
	7	8.78 ± 1.22
b. 1000 V		
	3	5.62 ± 1.10
	4	5.34 ± 0.57
	5	8.67 ± 0.48
	6	8.55 ± 0.26
	7	7.54 ± 0.24

ratios and table 4.9 the production cross section ratios normalized per unit energy interval obtained from the number of Rydberg electrons that are stripped at the entrance of the ionizer and inside the ionizer, respectively.

Rydberg electrons that are stripped at the entrance of the ionizer come from higher lying n-states of the ion than Rydberg electrons that are stripped inside the ionizer. With 1000 V across the ionizer we find that single and double capture events lead to significantly lower ratios than single excitation and excitation plus ionization events. With 500 V across the ionizer we find a similar

TABLE 4.9

RATIO OF RYDBERG ELECTRON PRODUCTION CROSS SECTIONS FOR RYDBERG ELECTRONS STRIPPED AT THE ENTRANCE OF THE IONIZER COMPARED TO RYDBERG ELECTRONS STRIPPED INSIDE THE IONIZER, NORMALIZED PER UNIT ENERGY INTERVAL

	q	ratios
a. 500 V		
	3	0.58 ± 0.20
	4	0.64 ± 0.13
	5	1.03 ± 0.18
	6	0.77 ± 0.11
	7	0.92 ± 0.13
b. 1000 V		
	3	0.60 ± 0.12
	4	0.59 ± 0.06
	5	0.95 ± 0.05
	6	0.91 ± 0.03
	7	0.81 ± 0.03

result, but our ratios have much larger experimental uncertainties. Again, assuming that the production cross sections per unit energy interval scale as n^{-3}, we expect these ratios to be ≈ 1. In table 4.9 we see that the ratios determined from projectile ionization events are close to one. However, the ratios that are determined from capture events are significantly less than one.

We find fewer electrons in the highest lying Rydberg states than electrons in somewhat lower lying Rydberg states for single and double capture events as opposed to

excitation and excitation plus ionization events. Capture to the highest lying Rydberg states is suppressed compared to capture to lower lying Rydberg states, and the cross sections for capture to very high Rydberg states do not scale as n^{-3}.

However, we find no significant difference in the ratios of the cross sections $\sigma(q+)_{1000}/\sigma(q+)_{500}$ normalized per unit energy interval if only a single target electron is transferred to a high Rydberg state of the projectile, or if in addition a second target electron is captured into a lower lying bound state of the projectile. Similarly, we find no significant difference in the same ratios if one projectile electron gets excited to a high Rydberg state of the projectile, or if in addition one or two projectile electrons are ionized. Within our experimental error the n-state distribution of high Rydberg states that are produced in an ion-atom collision is independent of the number of active electrons, but depends on whether electron capture or electron loss is responsible for the production process.

C. CONCLUSIONS

We have measured the production probabilities for Rydberg electrons stripped from very high Rydberg states of the projectile ion and for Rydberg electrons stripped from somewhat lower lying Rydberg states of the projectile ion. We have determined that the n-state distribution of these

Rydberg electrons is independent of whether the production process is single target electron capture to a high Rydberg state or target electron capture to a high Rydberg state plus capture to a lower lying bound state, and whether the event is single electron excitation to a high Rydberg state or excitation plus ionization. Capture events involving two active electrons and excitation events involving two active electrons lead to the same cross section ratios normalized per unit energy interval as capture and excitation events involving one active electron, respectively. Any correlation effects involving two active electrons in the production of these Rydberg states are not noticeable in the cross section ratios normalized per unit energy interval, within experimental error.

The production cross section ratios normalized per unit energy interval for electrons stripped from the highest lying Rydberg states of the projectile compared to electrons stripped from somewhat lower lying Rydberg states of the projectile are noticeably different for target electron capture to a high Rydberg state with or without an additional bound state capture as opposed to projectile electron excitation to a high Rydberg state with or without an additional ionization. The n-state distribution of the Rydberg electrons is dependent on the production mechanisms, i.e. if the Rydberg states are formed by target electron capture events or projectile electron excitation events.

It is possible that the difference in the n-state distribution can, at least partially, be attributed to the large momentum transfer that takes place during a close collision, which is necessary for capturing a target electron into a high Rydberg state of the projectile. The strong perturbation effecting the Coulomb field of the projectile ion by the ionized target atom may prevent target electron capture to the highest lying Rydberg states of the projectile. In support of this idea Underwood[12] measured a higher cusp electron to Rydberg electron ratio if the cusp and Rydberg electrons are produced by a target electron capture process as opposed to a projectile electron ionization process. For target electron capture events transferred electrons are more readily found in low lying continuum states of the projectile rather than in the highest lying Rydberg states of the projectile.

To gain a more thorough understanding of the processes that lead to the production of high Rydberg states in ion-atom collisions this experiment needs to be followed up by other experiments. The collision system in our experiment is very complex involving a multi-electron projectile as well as a multi-electron target. The use of a simpler projectile would be desirable. In addition a variety of noble gas targets should be used to investigate target-specific effects.

Modifying the ionizer used in this experiment can

provide several advantages. The difference in the radii of the inner and outer sectors of our ionizer is currently 2.54 cm. Increasing the difference will reduce effects of the fringe field near the entrance and exit apertures, and allow us to strip Rydberg electrons from a larger band of n-levels inside the ionizer. Using higher voltages across the ionizer will allow us to detect lower lying Rydberg states of the projectile. We then can compare the production cross sections for Rydberg electrons in the highest lying n-states of the projectile to those for Rydberg electrons in much lower n-states than is possible in this experiment.

In order to determine the detailed nature of the production of these high Rydberg states it will be necessary to examine many systems. Experiments at fast, intermediate, and slow collision velocities will have to be performed for complex as well as simple systems to support or disqualify the results presented here. If it is found that capture to the highest lying Rydberg state is suppressed, then it will have to be taken into account in ion-atom as well as ion-solid collisions.[27]

LIST OF REFERENCES

REFERENCES

1. W. Fritsch, and C. D. Lin, Phys. Rev. A 41, 4776 (1990).

2. M. Meron, and B. M. Johnson, Phys. Rev. A 41, 1365 (1990).

3. I. Shimamura, C. J. Noble, and P. G. Burke, Phys. Rev. A 41, 3545 (1990).

4. C. Fabre, S. Haroche, Rydberg States of Atoms and Molecules, eds. R. F. Stebbings and F. B. Dunning (Cambridge University Press, Cambridge, 1983) p.117.

5. M. R. C. McDowell, J. P. Coleman, Introduction to the Theory of Ion-Atom Collisions (North Holland, Amsterdam, 1970).

6. D. Kleppner, M. G. Littman, and M. L. Zimmerman, Sci. Am. 5, 244 (1981).

7. J. Macek, and M. E. Rudd, Case Stud. At. Mol. Phys. 3, 47 (1972).

8. J. Macek, Phys. Rev. A 1, 235 (1970).

9. J. H. McGuire, Phys. Rev. A 36, 1114 (1987).

10. L. H. Andersen, P. Hvelplund, H. Knudsen, S. P. Möller, and A. H. Sörenson, Phys. Rev. A 36, 3612 (1987).

11. J. H. McGuire, E. Salzborn, and A. Müller, Phys. Rev. A 35, 3265 (1987).

12. T. A. Underwood, Ph.D. Dissertation, University of Tennessee, (1990).

13. J. H. McGuire, J. Phys. B 17, L779 (1984).

14. R. R. Jones, and T. F. Gallagher, Phys. Rev. A 42, 2655 (1990).

15. R. D. DuBois, and Steven T. Manson, Phys. Rev. A 35, 2007 (1987).

16. E. Horsdal, B. Jenson, and K. O. Nielson, Phys. Rev. Lett. 57, 1414 (1986).

17. A. Müller, and E. Salzborn, Nucl. Instrum. Methods 164, 607 (1979).

18. J. P. Giese, M. Shulz, J. K. Swenson, H. Schöne, M. Benhenni, S. L. Varghese, C. R. Vane, P. F. Dittner, S. M. Shafroth, and S. Datz, Phys. Rev. A 42, 1231 (1990).

19. J. A. Tanis, G. Schiwietz, D. Schneider, N. Stolterfoht, W. G. Graham, H. Altevogt, R. Kowallik, A. Mattis, B. skoggvall, T. Schneider, and E. Szmola, Phys. Rev. A 39, Rapid Communications, 1571 (1989).

20. N. Stolterfoht, C. C. Havener, R. A. Phaneuf, J. K. Swenson, S. M. Shafroth, and F. W. Meyer, Phys. Rev. Lett. 57, 74 (1986).

21. E. P. Kanter, D. Schneider, Z. Vager, D. S. Gemmell, B. J. Zabransky, and Gu Yuan-zhuang, Phys. Rev. A 29, 583 (1984).

22. J. Stark, Ann. Physik 43, 965 (1914).

23. Daniel Kleppner, Francis M. Pipkin, The Spectroscopy of Highly Excited Atoms (Plenum Press, New York and London, 1977).

24. S. Haroche, Atomic Physics 7, eds. Daniel kleppner and Francis M. Pipkin (Plenum Press, New York and London, 1980) P.141.

25. E. M. Purcell, Phys. Rev. 54, 818 (1938).

26. H. A. Bethe, and E. E. Salpeter, Quantum Mechanics of One- and Two-Electron Atoms (Academic, New York, 1957).

27. Joachim Burgdörfer, in Transport Theory for Convoy Electrons and Rydberg Electrons in Solids, Lecture Notes in Physics Vol. 294, eds. D. Berényi, and G. Hock (Springer-Verlag, Hungary, 1987).

VITA

Brian Fitzgerald Hasson was born in Washington D.C. on September 30, 1964. He graduated from Rockville High School in Rockville Maryland, in May 1983. In May 1989, he received two Bachelor of Arts degrees; one in Mathematics, the other in Natural Science: primary concentration Physics, secondary concentration Biology, from ST. Mary's College of Maryland.

In December 1991, he will officially receive his Master of Science degree in Physics from the University of Tennessee. His MS work concentrated on experimental atomic collision physics and was conducted within the University of Tennessee Atomic Physics Group at the Oak Ridge National Laboratory EN Tandem Van de Graaff accelerator facility.